# A Multi-Loop Control Technique for the Stable Operation of Modular Multilevel Converters in HVDC Transmission Systems

Majid Mehrasa [a], Edris Pouresmaeil [b,c], Sasan Zabihi [d], Ionel Vechiu[c], and João P. S. Catalão [a,b,e,*]

[a] *C-MAST, University of Beira Interior, R. Fonte do Lameiro, 6201-001 Covilhã, Portugal*

[b] *INESC-ID, Instituto Superior Técnico, University of Lisbon, Av. Rovisco Pais, 1, 1049-001 Lisbon, Portugal*

[c] *ESTIA Institute of Technology, ESTIA, F-64210, Bidart, France*

[d] *ABB Australia Pty Limited, Berrimah, Northern Territory, Australia*

[e] *INESC TEC and Faculty of Engineering of the University of Porto, R. Dr. Roberto Frias, 4200-465 Porto, Portugal*

**Abstract:**

A multi-loop control strategy based on a six-order dynamic model of the modular multilevel converter (MMC) is presented in this paper for the high-voltage direct current (HVDC) applications. For the initial analysis of the operation of MMC, a capability curve based on active and reactive power of the MMC is achieved through a part of the six order dynamic equations. According to the MMC's control aims, the first loop known as the outer loop is designed based on passivity control theory to force the MMC state variables to follow their reference values. As the second loop with the use of sliding mode control, the central loop should provide appropriate performance for the MMC under variations of the MMC's parameters. Another main part of the proposed controller is defined for the third inner loop to accomplish the accurate generation of reference values. Also, for a deeper analysis of the MMC's dc link voltage stability, two phase diagrams of the dc-link voltage are assessed. Matlab/Simulink environment is used to thoroughly validate the ability of the proposed control technique for control of the MMC in HVDC application under both load and MMC's parameters changes.

***Index Terms*—**Modular multilevel converter (MMC); circulating currents; passivity control theory; sliding mode control; high-voltage direct current (HVDC).

# I. Nomenclature

| | | | |
|---|---|---|---|
| *Indices* | | OLC | Outer Loop Controller |
| *K* | *a, b, c* | SMs | Sub-Modules |
| *J* | *1,2* | LPF | Low Pass Filter |
| *Abbreviations* | | DLM | Direct Lyapunov Method |

* Corresponding author at Faculty of Engineering of the University of Porto.
*E-mail address:* catalao@ubi.pt (J.P.S. Catalão).

| | | | |
|---|---|---|---|
| KVL | Kirchhoff's Voltage Law | HVDC | High-Voltage, Direct Current |
| KCL | Kirchhoff's Current Law | MMCs | Modular Multilevel Converters |
| CLC | Central Loop Controller | PI | Proportional-Integral |
| ILC | Inner Loop Controller | SLPWM | Shift Level Pulse Width Modulation |

| | | | |
|---|---|---|---|
| $v_c$ | Rated capacitor voltage | *Variables* | |
| $S_{(ul)jk}$ | Switches of the MMCs | $Q_j^*$ | Reference values of Reactive power of MMCs |
| $v_{(ul)kj}$ | Lower and upper arms voltages | $H_{(dq)j}(s)$ | Transfer function |
| $v_{kj}$ | Output voltages of the MMCs | $Z_{dqj}$ | Error vector |
| $v_{dc}$ | *dc*-link voltage | $E_{dqj}$ | Total saved energy |
| $u_{kj1}$ | First equivalent modulation function of the respective SM stacks | $S_{dqj}$ | Time-variable sliding surface |
| $u_{kj2}$ | Second equivalent modulation function of the respective SM stacks | *Parameters* | |
| $v_{sm(ul)kj}$ | SMs voltages | $1/\xi_{(dq)}$ | Proportional gain |
| $v_{t(dq)j}$ | *ac*-side voltages of the MMCs | $L$ | Inductance of the MMCs |
| $v_{(dq)j}^*$ | Reference value of output voltages of the MMCs | $R$ | Resistance of the MMCs |
| $v_{dc}^*$ | Reference value of *dc*-link voltage | $L_p$ | Arm's inductance |
| $i_{kj}$ | Currents of MMCs | $R$ | Arm's resistance |
| $i_{cirkj}$ | Circulating currents of the MMCs | $C_{eq}$ | Equivalent *dc*-link capacitor |
| $i_{(ul)kj}$ | Lower and upper arms currents | $R_{dc}$ | Equivalent *dc*-link resistance |
| $i_{dcj}$ | MMCs *dc*-link currents | $R_{dq0j}$ | Injection resistances |
| $i_{sm(ul)kj}$ | Currents of SMs | $f_{ac}$ | *ac*-side frequency |
| $i_{(dq)j}^*$ | Reference values of MMCs currents | $f_s$ | Switching frequency |

| | | | |
|---|---|---|---|
| $i^*_{cir(dq)j}$ | Reference values of circulating currents | n | Numbers of SMs in each arm |
| $i_{l(dq)j}$ | Load currents | C | Capacitor of SM |
| $I_{av(dq)j}$ | Average currents of the MMCs | $C_{fi}$ | Capacitor of *ac* filter |
| $i_{(dq)\max j}$ | Maximum value of MMCs currents | $\omega_{(dq)2}, \omega_{(dq)\max 2}$ | Cut-off frequency |
| $\sum_{h=1}^{\infty} i_{l(dq)h}$ | Total harmonic current components of loads | $\omega_{p(dq)2} / \xi_{(dq)}$ | Integral gain |
| $P_j$ | Injected active power of MMCs | $k_{(dq)j}$ | Positive constant of CLC |
| $Q_j$ | Injected reactive power of MMCs | $\psi_{cir(dq)j}$ | Positive constant of CLC |
| $P^*_j$ | Reference values of active power of MMCs | $\psi_{(dq)j}$ | Positive constant of CLC |

# II. Introduction

The modular multilevel converter (MMC) topology has been a subject of increasing importance because of its special characteristics such as easy replacement of fault sub-modules (SMs), centralizing the distributed energies, modular structure, very low harmonic components and power losses, and also decreased rating values [1]-[5]. The MMCs have been widely utilized in various voltage/power levels of growing applications such as solar photovoltaic [6], large wind turbines [7-8], *ac* motor drives [9-10], high-voltage direct current (HVDC) transmission systems [11-12], *dc-dc* transformers [13], battery electric vehicles [14], distributed energy resources (DERs) [15-16], and flexible *ac* transmission systems (FACTS) [17].

Many researchers have focused on the control and modelling issues of the MMCs in various applications in recent years. Reference [18] deals with the fault condition of the MMC and tries to provide normal performance for the MMCs by the help of an energy-balancing control. A binary integer programming based model predictive control for the MMCs is proposed in [19] to optimize the multi-objective problem with minimum computing effort related to the control method which is the main contribution of the paper. A closed loop-needless PID controller along with increasing the arm inductance are considered to evaluate the effects of output voltage and current total harmonic distortion (THD) response in a modular multilevel converter [20]. Reference [21] presents a control strategy based on calculating the differential current references to provide desired operation for the MMCs in HVDC applications. Various dynamic models of the MMCs and their limitations in presenting robust control methods for these converters are investigated in [22]. In this paper, a complete derivation of the proposed switching state functions without losing any circuital characteristics of the converter is accomplished and a switching-cycle control approach proposed based on unused switching states of the MMCs. A modulation technique is proposed in [23] based

on a fixed pulse pattern fed into the SMs to maintain the stability of the stored energy in each SM, without measuring capacitor voltages or any other sort of feedback control. It also removes certain output voltage harmonics at any arbitrary modulation index and any output voltage phase angle. A current control design for independent adjustment of several current components and a systematic identification of current and voltage components for balancing the energy in the arms of an MMC is presented in [24]. In [25], a control strategy based on adding a common zero-sequence voltage to the reference voltages is proposed for balancing the arm currents of the MMCs under unbalanced load conditions. To reach it, a relationship between the dc-link active power and ac-link average active power is achieved and then, the dc component of the arm current is calculated through the ac-link average active power in the corresponding phase [25]. In the medium voltage systems, the energy storage can be embedded in MMC that causes several SMs to operate at significantly lower voltages [26]. In the structure presented in [27], the low-frequency components of the SM's output currents are removed by utilizing the interfaced batteries through the non-isolated dc/dc converters. Control algorithms proposed in this paper are developed to balance the state of charge of batteries. A compact and clear representation of differential equations is obtained for the MMC by introducing two nonlinear coordinate transformations in [28]. In the proposed model, two candidate outputs leaded to the internal dynamics of second or third order and a quasi-static feedback generates a linear input-output behaviour. Other different aspects of MMC application in HVDC system such as DC fault and DC solid-state transformers operating conditions are assessed in the references of [31]-[34].

In many existing methods, simultaneously having robustness against MMC parameters changes and also having very good dynamic tracking responses against the MMC's load changes have not been considered in their designed control techniques. But, in this paper, a multi-loop control strategy is aimed at providing a stable operation of the MMCs in HVDC application under both MMC's arm inductance and resistance parameters variations and also loads changes as well. This the first feature of the proposed controller that can increase the stability margins of the MMC performance with existence of more variations. According to the achieved six order dynamic equations of the MMCs, firstly the outer loop formed by passivity based control technique is introduced to enable the convergence ability of the MMC's state variables for its reference values in dynamic changes. Then, sliding mode controller is used to prepare the MMCs for stable operation against the MMC's parameters variations as the central loop of the proposed controller. The inner loop is employed to help other loops have accurate reference values for its used state variables that as another feature of the proposed controller, can generate instantaneously the needed references values of both MMCs in various operating conditions. Also, a capability curve is obtained to specify the allowable area of the MMC's active and reactive power generation in HVDC application and also R and L variations effects on the curve are evaluated that can provide some control considerations to understand more about the simulation results of the MMC's performance. Stability analysis of dc-link voltage is done in final part of this paper. Simulation results executed by Matlab/Simulink demonstrate the validity of the proposed control strategy in all operating conditions.

# III. The Proposed Differential Equation of MMC

Fig. 1(a) shows the proposed HVDC system which is consisted of two back-to-back MMCs. The *ac*-side of the MMC1 comprises *ac*-system-1, a line with inductance of $L$ and resistance of $R$, a three-phase step-down transformer and the input inductance and resistance of the MMC1. DC power is produced by MMC1 and then MMC2 uses this power to act as an inverter in HVDC structure. The resistance of $R_{dc}$ represents total switching loss of MMCs which is paralleled with dc link. The *ac*-side of the MMC2 consists of the output inductance and resistance, an *ac* filter to trap dominant switching harmonics, a load and a three-phase step-up transformer. The employed MMCs are shown in Fig. 1(b). A half-bridge converter is the same SM in which three states are appeared for each SM as: (1) switch $S_{(ul)kj1}$ is ON ($S_{(ul)kj2} \equiv off$), in which the output voltage of the SM is equal to $v_{sm(ul)kj}$, (2) switch $S_{(ul)kj2}$ is ON ($S_{(ul)kj1} \equiv off$) and consequently the SM's voltage becomes zero, and (3) as standby state, both upper and lower switches are not controlled ($S_{(ul)kj1} \equiv S_{(ul)kj2} \equiv off$) and the capacitor of SM is pre-charged. Two first states will be considered in this paper.

**Fig. 1(a) & Fig. 1(b)**

*A. Proposed six order dynamic model of MMCs*

It can be realized from Fig. 1(b) that the capacitor voltages of SM play a key role at generating dc-link voltage. Consequently, to regulate dc link voltage, $v_{(ul)kj}$ should be accurately controlled. The dynamic equation based on the MMC's currents can be achieved by the use of the Kirchhoff's voltage law (KVL) for Fig. 1(b) as,

$$v_{kj} + L\frac{di_{kj}}{dt} + Ri_{kj} + L_p\frac{di_{ukj}}{dt} + R_p i_{ukj} - \frac{v_{dc}}{2} + v_{ukj} = 0 \tag{1}$$

$$v_{kj} + L\frac{di_{kj}}{dt} + Ri_{kj} - L_p\frac{di_{lkj}}{dt} - R_p i_{lkj} + \frac{v_{dc}}{2} - v_{lkj} = 0 \tag{2}$$

The MMC currents based dynamic model can be driven by summing up (1) and (2) as,

$$\left(L + \frac{L_p}{2}\right)\frac{di_{kj}}{dt} + \left(R + \frac{R_p}{2}\right)i_{kj} + v_{kj} + u_{kj1} = 0 \tag{3}$$

where, $u_{kj1}$ can be calculated as,

$$u_{kj1} = \frac{\left(v_{ukj} - v_{lkj}\right)}{2} \tag{4}$$

To properly control the MMC currents for reaching desired values of active and reactive power sharing, dc-link voltage and SM voltages, the switching function of (4) is employed. Next important goal is decreasing the circulating currents of the MMCs which can be written as,

$$i_{cirkj} = \frac{i_{ukj} + i_{lkj}}{2} - \frac{i_{dcj}}{3} \tag{5}$$

The power losses of MMCs, the ripple magnitude of capacitor voltages and the total MMCs cost are increased because of existing circulating currents. By subtracting (1) from (2) and using (5), the circulating currents based differential equations can be achieved as (6),

$$L_p \frac{di_{cirkj}}{dt} + R_p i_{cirkj} + R_p \frac{i_{dcj}}{3} - \frac{v_{dc}}{2} + u_{kj2} = 0 \tag{6}$$

where, $u_{kj2}$ is defined as,

$$u_{kj2} = \frac{\left(v_{ukj} + v_{lkj}\right)}{2} \tag{7}$$

According to points of A and B in Fig. 1(b), the connection amid dc link voltage dynamic and MMC's arms currents is given as,

$$C_{eq} \frac{dv_{dc}}{dt} + \frac{v_{dc}}{R_{dc}} + \sum_{k=a}^{b,c} i_{uk1} + \sum_{k=a}^{b,c} i_{uk2} = 0 \tag{8}$$

$$C_{eq} \frac{dv_{dc}}{dt} + \frac{v_{dc}}{R_{dc}} + \sum_{k=a}^{b,c} i_{lk1} + \sum_{k=a}^{b,c} i_{lk2} = 0 \tag{9}$$

By summing up (8) and (9) and using (5), dc link voltage dynamic can be written in terms of dc link and circulating currents as (10),

$$C_{eq} \frac{dv_{dc}}{dt} + \frac{v_{dc}}{R_{dc}} + \sum_{k=a}^{b,c} i_{cirkj} + i_{dc1} + i_{dc2} = 0 \tag{10}$$

Noting the switching states of SMs, the dynamics of voltage of SMs for the lower and upper arms can be summarized as,

$$C \frac{dv_{sm(ul)kj}}{dt} = \begin{cases} i_{(ul)kj} & S_{(ul)kj1} \equiv on \\ i_{sm(ul)kj} \to 0 & S_{(ul)kj1} \equiv off \end{cases} \tag{11}$$

According to (11), and considering an appropriate approximation for the operation of the symmetrical voltages of capacitors of SMs in two arms, dynamic of output voltage of SMs can be deduced through the MMCs or circulating currents. It leads that the proposed controller effectively be involved in an effective balanced condition for the SMs capacitors in different operating

conditions. By transforming equations (3), (6) and (10) into dq reference frame, the proposed six order dynamic model of the MMCs in HVDC applications can be driven as,

$$\left(L+\frac{L_p}{2}\right)\frac{di_{dj}}{dt}+\left(R+\frac{R_p}{2}\right)i_{dj}-\omega\left(L+\frac{L_p}{2}\right)i_{qj}+u_{dj1}+v_{dj}=0 \tag{12}$$

$$\left(L+\frac{L_p}{2}\right)\frac{di_{qj}}{dt}+\left(R+\frac{R_p}{2}\right)i_{qj}+\omega\left(L+\frac{L_p}{2}\right)i_{dj}+u_{qj1}+v_{qj}=0 \tag{13}$$

$$L_p\frac{di_{cirdj}}{dt}+R_p i_{cirdj}-\omega L_p i_{cirqj}+u_{dj2}=0 \tag{14}$$

$$L_p\frac{di_{cirqj}}{dt}+R_p i_{cirqj}+\omega L_p i_{cirdj}+u_{qj2}=0 \tag{15}$$

$$L_p\frac{di_{cir0j}}{dt}+R_p i_{cir0j}+u_{0j2}-\frac{3\sqrt{2}v_{dc}}{2}+\sqrt{2}R_p i_{dcj}=0 \tag{16}$$

$$C_{eq}\frac{dv_{dc}}{dt}+\frac{v_{dc}}{R_{dc}}+\left(i_{cirdj}+i_{cirqj}+i_{cir0j}\right)+i_{dc1}+i_{dc2}=0 \tag{17}$$

*B. Capability Curve Analysis of MMCs Active and Reactive Power*

The MMC's potential in injection of maximum power is presented in this section. Based on Fig. 1(b), the MMCs dc-link and the ac side voltages are related to each other in d-q reference frame according to following equation,

$$v_{dc}i_{dcj}=v_{dtj}i_{dj}+v_{qtj}i_{qj} \tag{18}$$

By considering Fig. 1(b) and applying KVL's law to the ac side of the proposed MMC based HVDC system, the relation between the output and ac-side voltages of the MMC in dq reference frame can be achieved as,

$$v_{dtj}=v_{dj}+L\frac{di_{dj}}{dt}+Ri_{dj}-\omega Li_{qj} \tag{19}$$

$$v_{qtj}=v_{qj}+L\frac{di_{qj}}{dt}+Ri_{qj}+\omega Li_{dj} \tag{20}$$

By substituting (19) and (20) in (18) and also assuming $di_{(dq)j}/dt=I_{av(dq)}$, the following equation of a circle is driven as,

$$\left(i_{dj}+\frac{LI_{avdj}+v_{dj}}{2R}\right)^2+\left(i_{qj}+\frac{LI_{avqj}+v_{qj}}{2R}\right)^2=\frac{\left(LI_{avdj}+v_{dj}\right)^2+\left(LI_{avqj}+v_{qj}\right)^2+4Rv_{dc}i_{dcj}}{4R^2} \tag{21}$$

The (21) determines the operation area of MMC's currents in d-q reference frame. By considering the MMC's active and reactive power as $P_j=v_{dj}i_{dj}$ and $Q_j=-v_{dj}i_{qj}$ and substituting in (21), the power curve of MMC in the proposed HVDC system can be obtained as [29],

$$\left(P_j+\frac{LI_{avdj}v_{dj}+v_{dj}^2}{2R}\right)^2+\left(Q_j-\frac{LI_{avqj}v_{dj}+v_{dj}v_{qj}}{2R}\right)^2=\frac{\left(LI_{avdj}v_{dj}+v_{dj}^2\right)^2+\left(LI_{avqj}v_{dj}+v_{qj}v_{dj}\right)^2+4Rv_{dc}i_{dcj}v_{dj}^2}{4R^2} \quad (22)$$

The power curve of the proposed MMC based HVDC system in (22) is drawn in Fig. 2(a). It can be understood from this figure that the maximum and minimum amount of the MMC's active and reactive power are completely dependent on MMC's output parameters and also operation of the proposed MMC through the proposed controller. According to this figure, the center and radius of the power curve are definitely changed by MMC's output parameters, dc link specifications and also output currents and voltages of MMC in d-q reference frame. Fig. 2(b) and Fig. 2(c) show the various parameters effects of the MMC on the power curve. As can be seen, increasing the MMC's resistance (R) causes the power curve to become smaller with decreasing the radius and center. On the other hand, the scenario gets inverse when the MMC's inductance (L) increases as depicted in Fig. 2(c).

**Fig. 2**

# IV. Control Discussion

In this section, the sequent of designing process for the proposed multi-loop control technique is discussed in detail. The general aims of the proposed controller for the MMCs in HVDC applications are making stable operation under presence of both load and MMC's parameters changes that should be provided through the proposed three control loops i.e., outer, central and inner control loops (OLC, CLC, and ILC). OLC is aimed at leading the dynamic errors to attain zero value. The stable operation of the systems is assured with the CLC. Finally, the ILC provides reference currents for the both MMCs.

## *A. The Design of Outer Loop Controller (OLC)*

The outer loop controller is designed in this sub-section to provide the ability of tracking the reference values of the MMCs state variables for final proposed controller with the existence of load changes. The Passivity based control technique is used in this section. Firstly the proposed six order dynamic equation of (12)-(17) is presented as (23),

$$T_{dq0j}\frac{dQ_{dq0j}}{dt}+X_{dq0j}Q_{dq0j}+P_{dq0j}+O_{dq0j}+Y_{dq0j}=0 \quad (23)$$

All the matrixes used in (23) are presented in Appendix A. The proposed error vector of the MMCs is written as,

$$Z_{dq0j}=Q_{dq0j}-Q_{dq0j}^*=\left[i_{dj}-i_{dj}^* \quad i_{qj}-i_{qj}^* \quad i_{cirdj}-i_{cirdj}^* \quad i_{cirqj}-i_{cirqj}^* \quad i_{cir0j}-i_{cir0j}^* \quad v_{dc}-v_{dc}^*\right]^T \quad (24)$$

To reach an effective error vector for OLC, the main control aims of regulating MMC power, dc link voltage and ac voltages should be considered in calculating its reference values. Using (23) and (24), the description of MMC closed-loop error differential equation can be achieved as,

$$T_{dq0j}\frac{dZ_{dq0j}}{dt}+X_{dq0j}Z_{dq0j}=-Q_{dq0j}-Y_{dq0j}-P_{dq0j}-\left(T_{dq0j}\frac{dQ_{dq0j}^*}{dt}+X_{dq0j}Q_{dq0j}^*\right) \quad (25)$$

Based on passivity control theory, injecting series resistances to the MMC closed-loop error differential equation can significantly enhance the convergence rate of outer loop controller. Eq. (26) is used as series resistances,

$$R_{dq0j}=\begin{bmatrix} R_d & 0 & 0 & 0 & 0 & 0 \\ 0 & R_q & 0 & 0 & 0 & 0 \\ 0 & 0 & R_{cird} & 0 & 0 & 0 \\ 0 & 0 & 0 & R_{cirq} & 0 & 0 \\ 0 & 0 & 0 & 0 & R_{cir0} & 0 \\ 0 & 0 & 0 & 0 & 0 & \left(R_{dc}\right)^{-1} \end{bmatrix} \tag{26}$$

The completed closed-loop error differential equation of MMC can be obtained by adding the term of $R_{dq0j}Z_{dq0j}$ into the both sides of (25) as,

$$T_{dq0j}\frac{dZ_{dq0j}}{dt}+X_{dq0j}Z_{dq0j}+R_{dq0j}Z_{dq0j}=-Q_{dq0j}-Y_{dq0j}-P_{dq0j}-\left(T_{dq0j}\frac{dQ^{*}_{dq0j}}{dt}+X_{dq0j}Q^{*}_{dq0j}-R_{dq0j}Z_{dq0j}\right) \tag{27}$$

The desired operation of outer loop controller can be achieved by $Z_{dq0j}\to 0$. Thus,

$$T_{dq0j}\frac{dZ_{dq0j}}{dt}+X_{dq0j}Z_{dq0j}+R_{dq0j}Z_{dq0j}=0 \tag{28}$$

By applying (28) into (27), the proposed state variable error-based equation of outer loop controller can be obtained as,

$$-Q_{dq0j}-Y_{dq0j}-P_{dq0j}-\left(T_{dq0j}\frac{dQ^{*}_{dq0j}}{dt}+X_{dq0j}Q^{*}_{dq0j}-R_{dq0j}Z_{dq0j}\right)=0 \tag{29}$$

Equation (29) is used to reach the usable modulation functions of MMCs in outer loop controller as (30).

$$P_{dq0j}=\left[-Q_{dq0j}-Y_{dq0j}-\left(T_{dq0j}\frac{dQ^{*}_{dq0j}}{dt}+X_{dq0j}Q^{*}_{dq0j}-R_{dq0j}Z_{dq0j}\right)\right] \tag{30}$$

The Direct Lyapunov control theory is employed to prove that the proposed MMC's closed-loop error differential equation of OLC is stable. Thus, the Lyapunov function can be defined as,

$$\begin{aligned} E_{dq0j}\left(Z_{dq0j}\right)=&\frac{1}{2}\left(L+\frac{L_p}{2}\right)\left(z_{dj}\right)^2+\frac{1}{2}\left(L+\frac{L_p}{2}\right)\left(z_{qj}\right)^2+\frac{1}{2}L_p\left(z_{cirdj}\right)^2+\frac{1}{2}L_p\left(z_{cirqj}\right)^2 \\ &+\frac{1}{2}L_p\left(z_{cir0j}\right)^2+\frac{1}{2}C_{eq}\left(z_{dc}\right)^2 \end{aligned} \tag{31}$$

The error variables of z are the same defined in (24). To prove the globally asymptotic stability of (31) against the undesirable disturbances, the derivative of (31) in the state variables trajectories should definitively be negative. Therefore,

$$\frac{dE_{dq0j}}{dt}\left(Z_{dq0j}\right)=\left(L+\frac{L_p}{2}\right)\frac{dz_{dj}}{dt}z_{dj}+\left(L+\frac{L_p}{2}\right)\frac{dz_{qj}}{dt}z_{qj}+L_p\frac{dz_{cirdj}}{dt}z_{cirdj}+L_p\frac{dz_{cirqj}}{dt}z_{cirqj}$$
$$+L_p\frac{dz_{cir0j}}{dt}z_{cir0j}+C_{eq}\frac{dz_{dc}}{dt}z_{dc}=T_{dq0j}\frac{dZ_{dq0j}}{dt}Z_{dq0j}=-\left(X_{dq0j}Z_{dq0j}+R_{dq0j}Z_{dq0j}\right)Z_{dq0j} \quad (32)$$

The error variables based equation of (28) can be used to demonstrate that the terms generated by injection resistances in (32) are more dominant than other terms. Consequently, (32) can be summarized as,

$$\frac{dE_{dq0j}}{dt}\left(Z_{dq0j}\right)=-R_{dq0j}Z_{dq0j}Z_{dq0j}=-R_{dj}\left(z_{dj}\right)^2-R_{qj}\left(z_{qj}\right)^2-R_{cirdj}\left(z_{cirdj}\right)^2-R_{cirqj}\left(z_{cirqj}\right)^2$$
$$-R_{cir0j}\left(z_{cir0j}\right)^2-\left(R_{dcj}\right)^{-1}\left(z_{dcj}\right)^2<0 \quad (33)$$

The global asymptotical stability of the proposed outer loop controller can be guaranteed by (33). The proposed outer loop controllers of both MMCs used in HVDC system can be illustrated in Fig. 3. To regulate the MMCs currents for accurate active and reactive power sharing, Fig. 3(a) is employed in OLC. On the other hand, to minimize the MMC circulating currents, Fig. 3(b) can be used in the global structure of the proposed outer loop controller.

**Fig. 3 (a) & Fig. 3(b)**

*B. Design of the Central Loop Controller (CLC)*

In order to design a central loop controller with robust features, sliding mode controller is used in this sub-section to make a stable controller against MMC parameters changes. A time-varying sliding surface is considered as (34),

$$S_{dq0j}\left(t,Z_{dq0j}\right)=\left(\frac{d}{dt}+k_{dq0j}\right)^{g_n-1}Z_{dq0j} \quad (34)$$

The arbitrary constant values of $k_{dq0j}$ help CLC have a faster reaction against any parameter change. By the help of (34) and also selecting the relative degree 1 for $i_{mj}$ and $i_{cirmj}$, MMCs and circulating currents can have the reference sliding surfaces of (35) and (36), respectively as,

$$S_{dqj1}\left(t,\mathrm{z}_{dqj}\right)=z_{(dq)j}=i_{(dq)j}-i^*_{(dq)j} \quad (35)$$

$$S_{dq0j2}\left(t,\mathrm{z}_{cirdq0j}\right)=z_{cir(dq0)j}=i_{cir(dq0)j}-i^*_{cir(dq0)j} \quad (36)$$

The derivative of the reference sliding surfaces should be considered to provide the desired motion for MMCs and circulating currents on the sliding surfaces. Consequently, (37) and (38) can be achieved as,

$$\frac{dz_{(dq)j}}{dt}=\frac{di_{(dq)j}}{dt}-\frac{di^*_{(dq)j}}{dt}=-\psi_{(dq)j}\,\mathrm{sgn}\left(z_{(dq)j}\right) \quad (37)$$

$$\frac{dz_{cir(dq0)j}}{dt}=\frac{di_{cir(dq0)j}}{dt}-\frac{di^{*}_{cir(dq0)j}}{dt}=-\psi_{cir(dq0)j}\,\mathrm{sgn}\left(z_{cir(dq0)j}\right) \tag{38}$$

Using the sign function and also choosing properly $\psi_{(dq)j}$ and $\psi_{cir(dq0)j}$, can lead to improving the operation of central loop controller against MMCs parameters. The global structure of the proposed central loop controller for both MMCs and circulating currents is shown in Fig. 4.

**Fig. 4(a) & Fig. 4(b)**

The Lyapunov function of (39) is introduced to evaluate the stability of the central loop controller performance by considering the sliding law of (35)-(38) as,

$$J_j(Q)=\frac{1}{2}\left(z_{dj}\right)^2+\frac{1}{2}\left(z_{qj}\right)^2+\frac{1}{2}\left(z_{cirdj}\right)^2+\frac{1}{2}\left(z_{cirqj}\right)^2+\frac{1}{2}\left(z_{cir0j}\right)^2 \tag{39}$$

The equation of (40) is achieved by differentiating (39) in the trajectories of MMCs and circulating currents as,

$$\begin{aligned}\frac{dJ_j(Q)}{dt}&=z_{dj}\frac{dz_{dj}}{dt}+z_{qj}\frac{dz_{qj}}{dt}+z_{cirdj}\frac{dz_{cirdj}}{dt}+z_{cirqj}\frac{dz_{cirqj}}{dt}+z_{cir0j}\frac{dz_{cir0j}}{dt}=-z_{dj}\psi_{dj}\,\mathrm{sgn}\left(z_{dj}\right)-z_{qj}\psi_{qj}\,\mathrm{sgn}\left(z_{qj}\right)\\&-z_{cirdj}\psi_{cirdj}\,\mathrm{sgn}\left(z_{cirdj}\right)-z_{cirqj}\psi_{cirqj}\,\mathrm{sgn}\left(z_{cirqj}\right)-z_{cir0j}\psi_{cir0j}\,\mathrm{sgn}\left(z_{cir0j}\right)\le 0\end{aligned} \tag{40}$$

Since $z_{xj}\,\mathrm{sgn}\left(z_{xj}\right)$ becomes positive or zero value in each condition, the equation of (40) is definitely negative or zero. Thus, according to direct Lyapunov method, the proposed sliding mode based loop controller has stable operation in all its operating conditions.

*C. The Design of Inner Loop Controller (ILC)*

As discussed, the MMC2 acts as an inverter and also is responsible to supply nonlinear loads connected to the ac side of the MMC2. The d and q components of nonlinear load currents can be expressed as,

$$i_{l(dq)}=I_{1dq}+\sum_{h=1}^{\infty}i_{l(dq)h} \tag{41}$$

The term of $I_{1dq}$ is the fundamental component of load currents in d and q reference frame that is dependent on the MMC's CC. To specify the maximum values of $I_{1dq}$ in which MMC is able to supply, the proposed CC can be used. If the total harmonic components of load currents in d-q reference frame are stated as (41),

$$\sum_{h=1}^{\infty}i_{l(dq)h}=i_{l(dq)}\left(1-\frac{\omega_{(dq)2}}{s+\omega_{(dq)2}}\right) \tag{42}$$

A LPF-based transfer function is used in (42) to obtain the harmonic components of load currents in the MMC2 side [30]. To perform a precise active and reactive power sharing of the MMC2, extracting properly the harmonic components is very important and thus an appropriate process of designing inner loop controller must be done as shown in Fig. 5(a). This figure is contained PI controllers as well as LPF in which their gains and cut-off frequency should be properly considered. The process of achieving the MMC1 reference values is illustrated in Fig. 5(b). As shown in Fig. 5(b), to complete the MMC1 reference values, the total reactive power of MMC1 loads $Q_{l2}$ is used.

**Fig. 5(a) & Fig. 5(b)**

# V. Convergence Evaluation and Stability Analysis

In this section, the ability of MMC2 in load compensation is investigated based on a transfer function established from the Fig. 5(a). Then, the *dc*-link voltage stability of the proposed model is assessed based on the dynamic equations obtained from Fig. 1(b).

## *A. The load compensation capability analysis of MMC2*

In order to evaluate the capability of MMC2 for tracking the reference current components in d-q frame, the ratio of $i_{dq2}$ and $i^*_{dq2}$ are defined as the objective functions. Following equations describe the relations between the load current and the maximum value of currents of the MMC2 at the fundamental frequency,

$$i_{ldq2} = \alpha i_{ldq2} \ , \ i_{\mathrm{dq\,max\,2}} = \beta \left( \frac{\omega_{\mathrm{dq\,max\,2}}}{s + \omega_{\mathrm{dq\,max\,2}}} \right) i_{dq2} \tag{43}$$

By combination of (43) and the equation obtained from Fig. 5(a), following transfer function can be achieved,

$$H_{dq2}(s) = \frac{i_{dq2}}{i^*_{dq2}} = \frac{\xi_{dq} s^3 + \xi_{dq}\left(\omega_{dq2} + \omega_{\mathrm{dq\,max\,2}}\right) s^2 + \xi_{dq}\omega_{dq2}\omega_{\mathrm{dq\,max\,2}} s}{\left( \begin{array}{l} (\alpha - 1) s^3 + \left( (\alpha + \beta)\omega_{\mathrm{dq\,max\,2}} - \left(\omega_{dq2} + \omega_{\mathrm{dq\,max\,2}}\right) + \omega_{pdq2}(\alpha - 1) \right) s^2 \\ + \left( (\beta - 1)\omega_{dq2}\omega_{\mathrm{dq\,max\,2}} + (\alpha + \beta)\omega_{pdq2}\omega_{\mathrm{dq\,max\,2}} - \omega_{pdq2}\left(\omega_{dq2} + \omega_{\mathrm{dq\,max\,2}}\right) \right) s \\ + (\beta - 1)\omega_{pdq2}\omega_{dq2}\omega_{\mathrm{dq\,max\,2}} \end{array} \right)} \tag{44}$$

Equation (44) can be used to specify appropriate values for the utilized LPF, PI controller gains, $\alpha$ and $\beta$. For a normal operation, the values of $\alpha$ and $\beta$ are almost in the range of 0 and 1, and also the LPF has the cut-off frequency of $\omega_{dq2} = \omega_{\mathrm{dq\,max\,2}} = 2\pi f_c \left( f_c = f_s / 2 \right)$, which promises the extraction of the *dc* part and also low harmonic components from the nonlinear load currents. Consequently, by analysing the transfer function of (44), the proportional and integral gains of the PI controller (i.e., $1/\xi_{dq}$ and $\omega_{pdq2}/\xi_{dq}$) can be calculated.

*B. Dynamic model analysis of the dc-link voltage*

Dynamic model analysis of the *dc*-link voltage is investigated to validate the appropriate performance of the proposed HVDC model shown in Fig. 1(b). By applying KCL's into the point A, following equation can be obtained [29],

$$C_{eq}\frac{dv_{dc}}{dt}=-\frac{v_{dc}}{R_{dc}}+i_{dc1}-i_{dc2} \tag{45}$$

The relationship between the MMCs *dc*-link and *ac* side voltages is presumed to be: $i_{dcj}v_{dc}=v_{dtj}i_{dj}+v_{qtj}i_{qj}$. Then, (45) can be rewritten as,

$$C_{eq}\frac{dv_{dc}}{dt}=-\frac{v_{dc}}{R_{dc}}+\frac{\left(v_{dt1}i_{d1}+v_{qt1}i_{q1}\right)-\left(v_{dt2}i_{d2}+v_{qt2}i_{q2}\right)}{v_{dc}} \tag{46}$$

By neglecting the instantaneous power on impedances of MMCs, the term $v_{dtj}i_{dj}+v_{qtj}i_{qj}$ is approximately equal to $v_{dj}i_{dj}$; and consequently, (46) can be simplified as,

$$C_{eq}\frac{dv_{dc}}{dt}=\frac{-v_{dc}^2+R_{dc}\left(P_1-P_2\right)}{R_{dc}v_{dc}} \tag{47}$$

The zero dynamic stability of (47) is studied to verify the internal stability of the proposed model. The zero dynamic value of *dc*-link voltage is obtained by $dv_{dc}^*/dt=0$. Therefore,

$$v_{dc}^*=\sqrt{R_{dc}^*\left(P_1^*-P_2^*\right)}=\sqrt{R_{dc}^*}\sqrt{\left(i_{d1}^*v_{d1}^*-i_{d2}^*v_{d2}^*\right)} \tag{48}$$

Equation (48) confirms that the desired value of *dc*-link voltage does entirely rely on the accurate control of active power for the MMCs. In addition to the precise values for the d-component of MMCs currents, the output *ac* voltages of MMCs required to be finely regulated in order to achieve a desired *dc*-link voltage. To plot the phase diagram of the *dc*-link voltage, (47) is rearranged as,

$$\frac{dv_{dc}}{dt}=\frac{-v_{dc}^2+R_{dc}\left(P_1-P_2\right)}{R_{dc}C_{dc}v_{dc}}=\frac{-v_{dc}^2+a}{bv_{dc}}$$
$$a=R_{dc}\left(P_1-P_2\right),b=R_{dc}C_{dc} \tag{49}$$

The phase diagrams for dynamic equation of the *dc*-link voltage are depicted in Fig. 6. As can be seen, the zero dynamic value of HVDC system *dc*-link voltage is completely stable in both states, which confirms that the proposed HVDC model reaches a desired *dc*-link voltage in different operation scenarios.

**Fig. 6(a) & Fig. 6(b)**

# VI. Results and Discussions

The ability of the proposed multi-loop controller is evaluated in this section. For this, a three-level MMC-HVDC system is considered based on the proposed model in Fig. 1(a) and is modelled in the Matlab/Simulink environment in discrete-time mode with sample time of $20\mu s$. Stringent and comprehensive simulation results are provided in this section, alongside a solid mathematical background, to validate operation of the proposed control technique in HVDC power system. Simulation results are presented in order to confirm high performance of the proposed control technique in *dc*-link voltage control, capacitor voltage balancing, and circulating current minimization. In addition, performance of the proposed MMC-based HVDC model in Fig. 1(a) including power and control subsystems are evaluated under various operating conditions. System parameters are provided in Table I and the schematic diagram and principle of the proposed control technique in MMC-HVDC system is shown in Fig. 7.

TABLE I

SIMULATION PARAMETERS

| | | | |
|---|---|---|---|
| $f_{ac}$ | 60 Hz | C | 25mF |
| $f_s$ | 10 kHz | $C_{fi}$ | 615μF |
| $v_{dc}$ | 42kV | $R_{dc}$ | 4kΩ |
| $v_c$ | 14kV | $P^{\mu},Q^{\mu}$ | 150MW ,75MVAR |
| $L_{jk}$ | 25mH | Transformer power rating | 23kV/130kV (Δ/Y) |
| $R_{jk}$ | 1Ω | load I of MMC1 | 65MW,-20MVAR |
| $L_k$ | 6mH | load II of MMC1 | 70MW,80MVAR |
| $R_k$ | 0.3Ω | load I of MMC2 | 20MW,7MVAR |
| n | 3 | load II of MMC2 | 30MW,20MVAR |
| Grid Resistance | 0.3 Ω | Dead Time | 20e-6 s |
| Grid Inductance | 3 mH | HVDC line Inductance | 10 mH |

**Fig. 7**

### *A. The load variations based assessment of the proposed control technique*

Dynamics and steady state responses of the proposed model including assigned parameter values in table I are evaluated in this subsection. The scenarios for evaluation of OLC and ILC performance during the load changes are defined as following. At the beginning, in the time interval of 0<t<1/2 sec, a 65MW-j20MVAR load and a 20MW+j7MVAR load are connected to the *ac*

sides of MMC1 and MMC2 respectively and the MMCs are supplying these loads in the steady state operating conditions. This process is continued up to t=1/2 sec where a step load increment is occurring for both MMCs so that in the time interval of 1/2<t<1 sec, a 70MW+j80MVAR load and a 30MW+j20MVAR load are added to the prior loads of MMC1 and MMC2 respectively. The phase "a" of the upper and lower switching functions of MMCs can be seen in Fig. 8. As it can be observed from this figure, the upper and lower switching functions of MMC2 experiences a little more transient response because of more responsibilities of MMCs in supplying load variations. These switching functions are employed for SLPWM of MMCs in HVDC system. Fig. 9 shows the *dc*-link voltage of the system, which is subject to the change of power demand. However as evident, it is regulated with minimum fluctuations (maximum 0.05 kV) around its nominal value at 42 kV. In addition, during the entire processing time, the SM capacitor voltages of both MMCs are kept balanced around their desired values of $v_{dc}/3$ ($V_{dc}$/N for N=3) with very low ripples considering its response to the power variations.

**Fig. 8**

**Fig. 9**

Fig. 10 shows three phase balanced *ac* voltages of MMCs in the proposed HVDC system in the steady state operating condition. As shown in this figure during load variations, the *ac* voltages of MMCs maintain sinusoidal waveforms without any noticeable distortions. The quality of the proposed control technique to minimize circulating currents of converter arms is demonstrated in Fig. 11. As given in the figure, the circulating currents of MMCs are reduced to small values during both dynamic and steady state operating conditions. The dynamic response of the proposed control technique to the step variations in active and reactive power commands is shown in Fig. 12. As it can be seen, MMC1 is almost set at the desired values with 65 MW and -20 MVAR. MMC2 produces the active power required for line resistances and nonlinear load I and also sinks the reactive power generated by the output filter to allow the voltage to settle the desired output voltages as depicted in Fig. 10. Injected active and reactive power from MMC1 follows the load power variations, which confirms merits of the proposed OLC and ILC closed-loop controllers in control of interfaced MMC in the proposed HVDC model.

Fig.12 indicates the capability of the proposed control technique to pursue a consecutive increment through MMC2 during the dynamic operating condition. As it can be seen, MMC2 is able to generate required active power of additional loads with a short transient time. Reactive power changes of MMC2 is proportional to output filter variations for reaching a balanced three phase voltage.

**Fig. 10**

**Fig. 11**

**Fig. 12**

*B. The parameter variations based assessment of the proposed control technique*

The designed central loop controller operation of the MMCs once dealing with the parameter change is evaluated in this subsection. Fig. 13 shows the changes in resistances and inductances of MMCs considered in this sub-section.

**Fig. 13**

Fig. 14 illustrates the upper and lower switching functions of the phase "a" of MMC1 and MMC2 under parameters changes. For both upper and lower switching functions, more transient state can be seen in the middle of the MMC's parameters changes and more stability is governed in the other time interval of MMC's parameters variations. The dc-link voltage of the proposed HVDC system and SM capacitor voltages of MMCs in presence of MMC parameters variations are depicted in Fig. 15. Based on this figure, the reference values can be followed by the proposed controller with allowable transient response which verifies the accurate operation of both designed CLC and ILC.

**Fig. 14**

**Fig. 15**

In this condition, three phase balanced ac voltages can be properly generated by MMCs as shown in Fig. 16. The MMCs circulating currents are shown in Fig. 17. According to this figure, the proposed controller is able to minimize MMCs circulating currents within acceptable values along with slight transient responses in the time of dynamic change.

In presence of parameters variations, the loads of 140MW+j45MVAR and 35MW+j25MVAR are supplied through MMC1 and MMC2, respectively as depicted in Fig. 18. As it can be observed from Fig. 18, the active and reactive power sharing of both MMCs can be accomplished. However, some slight changes happen for both active and reactive power of MMCs because of reactive and resistance variations that are located in acceptable range according to Fig. 18.

**Fig. 16**

**Fig. 17**

**Fig. 18**

# VII. Conclusion

A multi-loop control strategy for the stable operation of MMCs in HVDC system was proposed in this paper under both load and MMCs parameters variations. Firstly, a six-order dynamic equation was achieved for both MMCs and subsequently a curve based on active and reactive power of MMC was introduced to analyse in depth the MMCs capability of generating both powers. Based on this dynamic model, as the first advantage, a capability curve based on MMC active and reactive power was proposed and the R and L variations effects on the curve were assessed that could provide some control considerations to understand more about the simulation results of the MMC's performance. To design the first loop of the proposed controller, the passivity based control technique was employed to shape OLC for increasing the MMCs convergence ability in dynamic changes. In the next step, to add the robustness feature against MMCs parameters changes, the sliding mode controller was considered to shape the central loop controller. As the second important advantage of the proposed controller, the proposed controller was able to simultaneously being robustness against MMC´s arm inductance and resistance variations and also having very good dynamic tracking responses against the MMC's load changes. As the third feature of the proposed controller, accurate reference values for MMCs state variables were generated through the inner loop controller using appropriate LPF and regulated PI controllers that could generate instantaneously the requested references values of both MMCs in all considered operating conditions. To further analyse the MMC based HVDC system, the dc-link voltage stability analysis was also carried out. Finally, to confirm the validity of the proposed control technique, Matlab/Simulink was used to achieve stringent simulation results of MMCs based HVDC system under both load and MMCs parameters changes.

# Acknowledgment

This work was supported by INSUL'GRID project, France, by FEDER funds through COMPETE 2020 and by Portuguese funds through FCT, under Projects SAICT-PAC/0004/2015 - POCI-01-0145-FEDER-016434, POCI-01-0145-FEDER-006961, UID/EEA/50014/2013, UID/CEC/50021/2013, UID/EMS/00151/2013, and SFRH/BPD/102744/2014. Also, the research leading to these results has received funding from the EU Seventh Framework Programme FP7/2007-2013 under grant agreement no. 309048.

# Appendix

# Appendix A:

$$Q_{dq0j}=\begin{bmatrix} i_{dj} \\ i_{qj} \\ i_{cirdj} \\ i_{cirqj} \\ i_{cir0j} \\ v_{dc} \end{bmatrix}, T_{dq0j}=\begin{bmatrix} R+0.5R_p & 0 & 0 & 0 & 0 & 0 \\ 0 & R+0.5R_p & 0 & 0 & 0 & 0 \\ 0 & 0 & L_p & 0 & 0 & 0 \\ 0 & 0 & 0 & L_p & 0 & 0 \\ 0 & 0 & 0 & 0 & L_p & 0 \\ 0 & 0 & 0 & 0 & 0 & C_{eq} \end{bmatrix}$$

$$X_{dq0j}=\begin{bmatrix} \left(R+0.5R_p\right) & -\omega\left(L+0.5L_p\right) & 0 & 0 & 0 & 0 \\ \omega\left(L+0.5L_p\right) & \left(R+0.5R_p\right) & 0 & 0 & 0 & 0 \\ 0 & 0 & R_p & -\omega L_p & 0 & 0 \\ 0 & 0 & \omega L_p & R_p & 0 & 0 \\ 0 & 0 & 0 & 0 & R_p & -\dfrac{3\sqrt{2}}{2} \\ 0 & 0 & 1 & 1 & 1 & \dfrac{1}{R_{dc}} \end{bmatrix}$$

$$P_{dq0j}=\begin{bmatrix} u_{dj1} \\ u_{qj1} \\ u_{dj2} \\ u_{qj2} \\ u_{0j2} \\ 0 \end{bmatrix}, O_{dq0j}=\begin{bmatrix} 0 \\ 0 \\ 0 \\ 0 \\ \sqrt{2}R_p i_{dcj} \\ i_{dc1}+i_{dc2} \end{bmatrix}, Y_{dq0j}=\begin{bmatrix} v_{dj} \\ v_{qj} \\ 0 \\ 0 \\ 0 \\ 0 \end{bmatrix}$$

# References


[1] Lesnicar A, Marquardt R. An innovative modular multilevel converter topology suitable for a wide power range. In Proc. IEEE Bologna PowerTech Conference, 2003.

[2] Mehrasa M, Pouresmaeil E, Akorede M, Zabihi S, Catalão J P S. Function-Based Modulation Control for Modular Multilevel Converters under Varying Loading and Parameters Conditions. IET Generation, Transmission & Distribution, 2017; doi: 10.1049/iet-gtd.2016.1028.

[3] Fehr H, Gensior A, Muller M. Analysis and trajectory tracking control of a modular multilevel converter. IEEE Trans. Power Electron 2014; 30 (1): 398-407.

[4] Mehrasa M, Hosseini S K, Taheri S, Pouresmaeil E, Catalao J P S. Dynamic performance control of modular multilevel converters in HVDC transmission systems. IEEE Electrical Power and Energy Conference (EPEC), 2016.

[5] Ilves K, Antonopoulos A, Norrga S, Nee H-P. Steady-state analysis of interaction between harmonic components of arm and line quantities of modular multilevel converters. IEEE Trans. Power Electron 2012; 27(1): 57-68.

[6] Alexander A, Thathan M. Modelling and analysis of modular multilevel converter for solar photovoltaic applications to improve power quality. IET Renewable Power Generation 2015; 9(1): 78 - 88.

[7] Debnath S, Saeedifard M. A New Hybrid Modular Multilevel Converter for Grid Connection of Large Wind Turbines. IEEE Trans. Sustainable Energy 2013; 4 (4):1051 - 1064.

[8] Zhang Y, Ravishankar J, Fletcher J, Li R, Han M. Review of modular multilevel converter based multi-terminal HVDC systems for offshore wind power transmission. Renewable and Sustainable Energy Reviews In Press, Corrected Proof, Available online 8 February 2016.

[9] Antonopoulos A, Angquist L, Norrga S, Ilves K, Harnefors L, Nee H-P. Modular Multilevel Converter AC Motor Drives with Constant Torque From Zero to Nominal Speed. IEEE Trans. Industry Applications 2013; 50 (3): 1982 - 1993.

[10] Antonopoulos A, Angquist L, Harnefors L, Nee H-P. Optimal Selection of the Average Capacitor Voltage for Variable-Speed Drives With Modular Multilevel Converters. IEEE Trans. Power Electron 2014; 30 (1): 227 - 234.

[11] Nami A, Liang J, Dijkhuizen F, Demetriades G D. Modular Multilevel Converters for HVDC Applications: Review on Converter Cells and Functionalities. IEEE Trans. Power Electron 2014; 30 (1): 18 - 36.

[12] M Mehrasa, E Pouresmaeil, S Zabihi, JC Trujillo Caballero, JPS Catalão. A novel modulation function-based control of modular multilevel converters for high voltage direct current transmission systems. Energies 2016; 9 (11): 867-880.

[13] Gowaid I, Adam G, Ahmed S, Holliday D, Williams B. Analysis and Design of a Modular Multilevel Converter with Trapezoidal Modulation for Medium and High Voltage dc-dc Transformers. IEEE Trans. Power Electron 2015; 30 (10): 5439 - 5457.

[14] Quraan M, Yeo T, Tricoli P. Modular Multilevel Converters for HVDC Applications: Review on Converter Cells and Functionalities. IEEE Trans. Power Electron 2015; doi: 10.1109/TPEL.2015.2408435.

[15] Soong T, Lehn P W. Internal Power Flow of a Modular Multilevel Converter with Distributed Energy Resources. IEEE Journal of Emerging and Selected Topics in Power Electronics 2014; 2(4):1127 - 1138.

[16] Pouresmaeil E, Mehrasa M, Shokridehaki M A, Rodrigues E M G, Catalão J P S. Control of Modular Multilevel Converters for Integration of Distributed Generation Sources into the Power Grid. In Proc. SEGE 2015; 1-6.

[17] Du S, Liu J. A Study on DC Voltage Control for Chopper-Cell-Based Modular Multilevel Converters in D-STATCOM Application. IEEE Trans. Power Delivery 2013; 28 (4): 2030 - 2038.

[18] Debnath S, Jiangchao Q, Bahrani B, Saeedifard M, Barbosa P. Operation, Control, and Applications of the Modular Multilevel Converter: A Review. IEEE Trans. Power Electron 2014; 30 (1): 37 - 53.

[19] Disfani V R, Fan L, Miao Z, Ma Y. Fast model predictive control algorithms for fast-switching modular multilevel converters. Electric Power Systems Research 2015*;* 129: 105–113.

[20] Gebreel A A, Xu L. Power quality and total harmonic distortion response for MMC with increasing arm inductance based on closed loop-needless PID controller. Electric Power Systems Research 2016; 133: 281–291.

[21] Jiangchao Q, Saeedifard M. Predictive Control of a Modular Multilevel Converter for a Back-to-Back HVDC System. IEEE Trans. Power Delivery 2012; 27 (3): 1538 - 1547.

[22] Bergna G, Garces A, Berne E, Egrot P, Arzande A, Vannier J-C, Molinas. A Generalized Power Control Approach in ABC Frame for Modular Multilevel Converter HVDC Links Based on Mathematical Optimization. IEEE Trans. Power Delivery 2013; 29 (1): 386 - 394.

[23] Wang J, Burgos R, Boroyevich D. Switching-Cycle State-Space Modeling and Control of the Modular Multilevel Converter. IEEE Journal of Emerging and Selected Topics in Power Electronics 2014*;* 2 (4):1159 - 1170.

[24] Ilves K, Antonopoulos A, Norrga S, Nee H-P. A New Modulation Method for the Modular Multilevel Converter Allowing Fundamental Switching Frequency. IEEE Trans. Power Electron 2012*;* 27 (8): 3482 - 3494.

[25] Lia X, Songa Q, Liua W, Lia Q, Raob H, Xub S. Zero-sequence voltage injection control scheme of modular multilevel converter supplying passive networks under unbalanced load condition. Electric Power Systems Research 2015; 121: 270–278.

[26] Moon J W, Gwon J S, Park J W, Kang D W, Kim J M. Model Predictive Control With a Reduced Number of Considered States in a Modular Multilevel Converter for HVDC System. IEEE Trans. Power Delivery 2014*;* 30 (2): 608 - 617.

[27] Vasiladiotis M, Rufer A. Analysis and Control of Modular Multilevel Converters With Integrated Battery Energy Storage. IEEE Trans. Power Electron 2014; 30 (1):163 - 175.

[28] Barnklau H, Gensior A, Rudolph J. A Model-Based Control Scheme for Modular Multilevel Converters. IEEE Trans. Industrial Electron 201; 60 (12): 5359 - 5375.

[29] Mehrasa M, Pouresmaeil E, Zabihi S, Catalao J P S. Dynamic Model, Control and Stability Analysis of MMC in HVDC Transmission Systems. IEEE Trans. Power Delivery 2017; 32 (3): 1471 - 1482.

[30] Pouresmaeil E, Mehrasa M, Catalao J P S. A Multifunction Control Strategy for the Stable Operation of DG Units in Smart Grids. IEEE Trans. Smart grid 2015; 6 (2): 598 - 607.

[31] Li R, Fletcher, J E. A novel MMC control scheme to increase the DC voltage in HVDC transmission systems. Electric Power Systems Research 2017; 143: 544-553.

[32] Li R, Fletcher J E, Xu L, Williams B W. Enhanced Flat-Topped Modulation for MMC Control in HVDC Transmission Systems. IEEE Transactions on Power Delivery 2017; 32(1): 152-161.

[33] Li R, Xu L, Yao L, Williams B W. Active Control of DC Fault Currents in DC Solid-State Transformers During Ride-Through Operation of Multi-Terminal HVDC Systems. IEEE Transactions on Energy Conversion 2016; 31(4): 1336-1346.

[34] Li R, Xu L, Holliday D, Page F, Finney S J, Williams B W. Continuous Operation of Radial Multiterminal HVDC Systems Under DC Fault. IEEE Transactions on Power Delivery 2016; 31(1): 351-361.

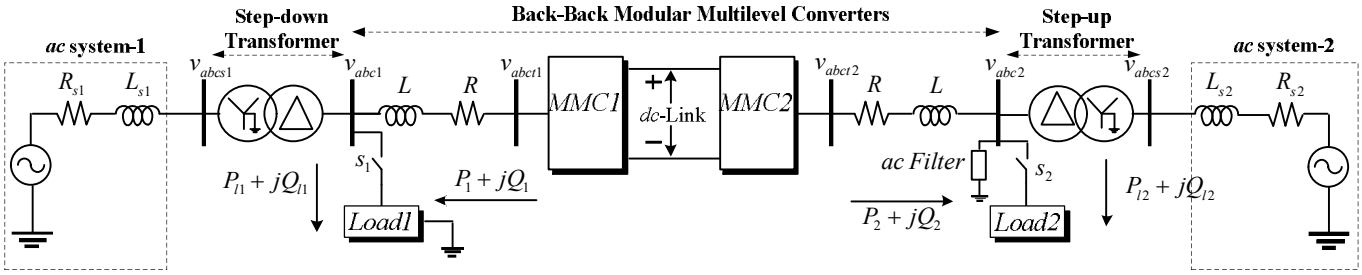


**(a)**

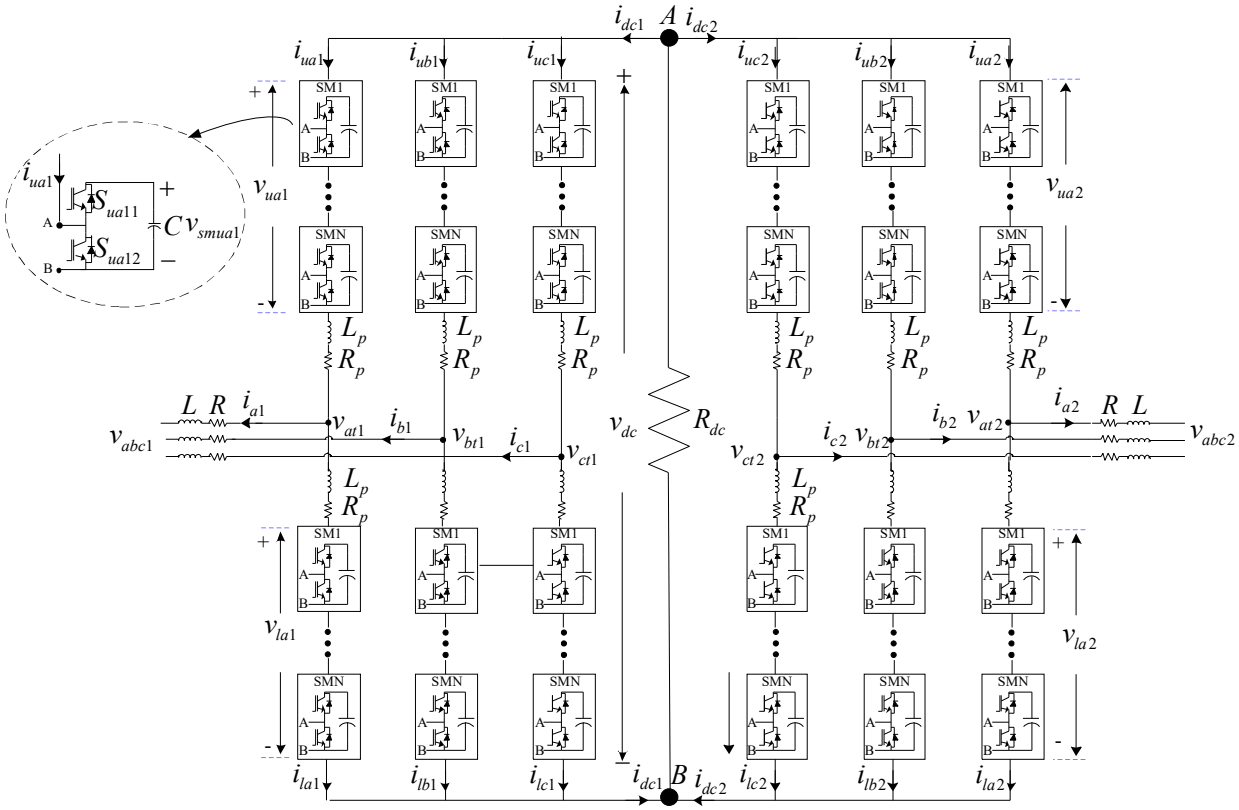


**(b)**

**Fig. 1. Schematic diagram of the MMC-HVDC system. (a) Single-line diagram model and (b) circuit diagram of the back-to-back MMC.**

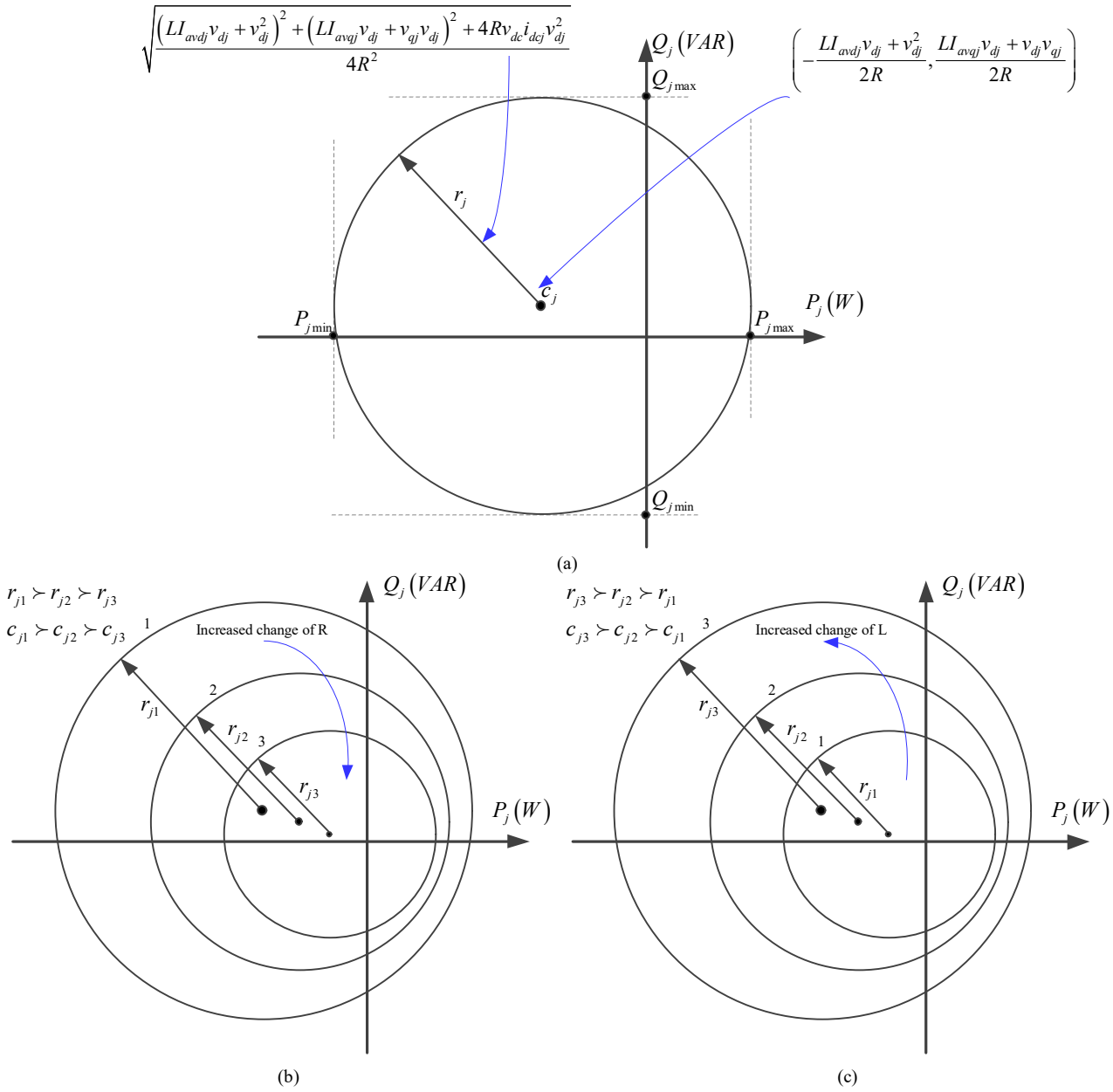


**Fig. 2. (a) Power curve of MMCs (b) R and L changes effects on MMCs power curve.**

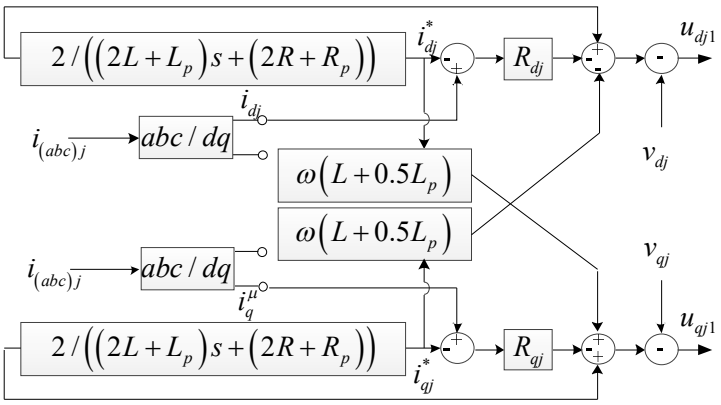


(a)

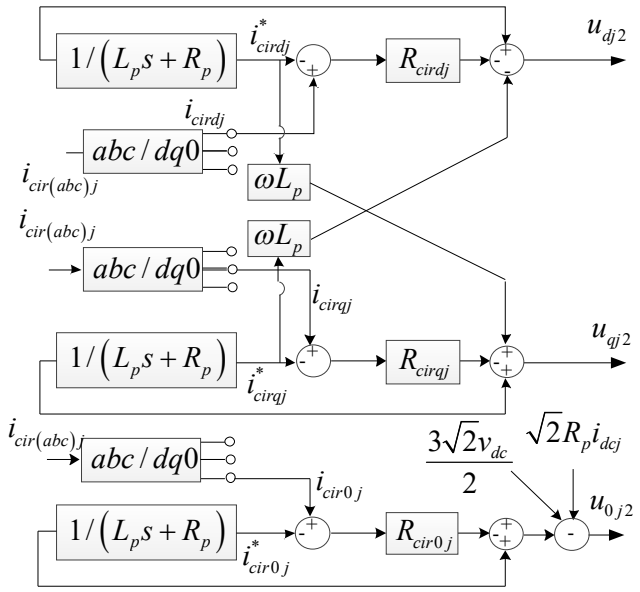


(b)

**Fig. 3. The proposed outer loop controller for (a) MMCs currents (b) MMCs circulating currents**

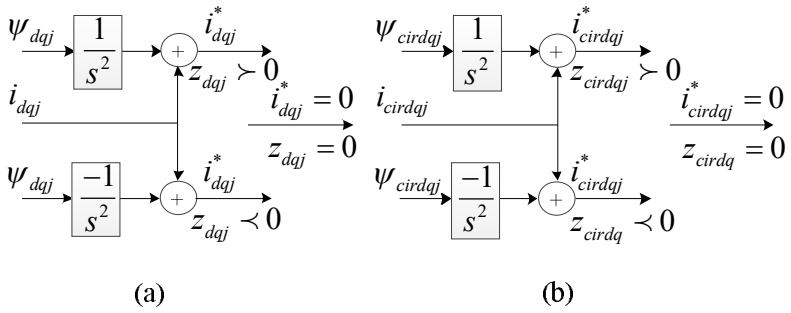


**Fig. 4. The Proposed Central Loop Controller for (a) MMCs currents (b) MMCs circulating currents.**

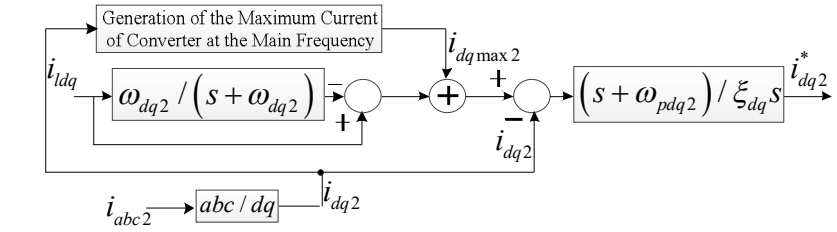


**(a)**

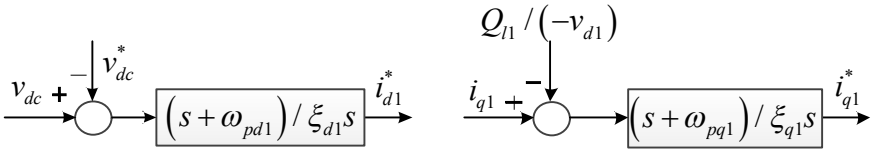


**(b)**

**Fig. 5. The Proposed Inner Loop Controller for (a) the MMC2 reference currents (b) the MMC1 reference currents.**

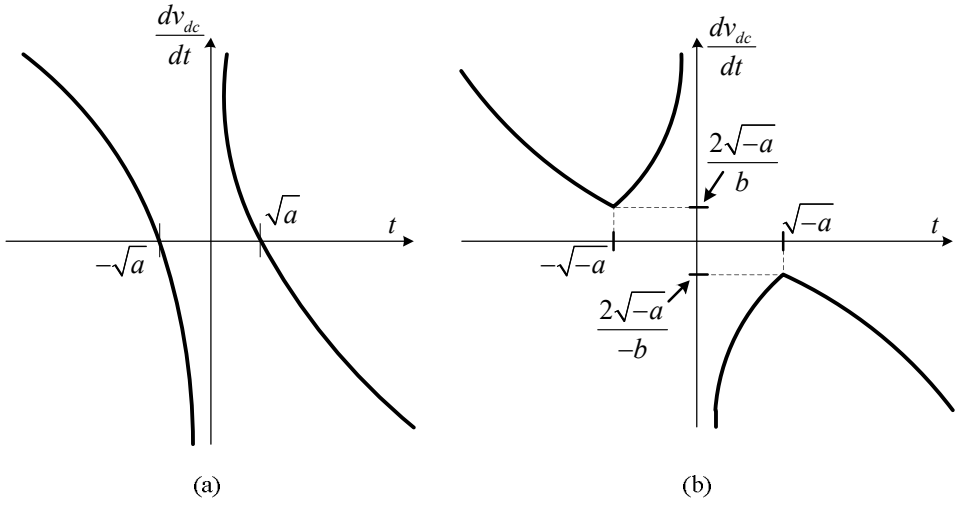


**Fig. 6. The phase diagrams of the *dc*-link voltage (a) a>0 and (b) a<0.**

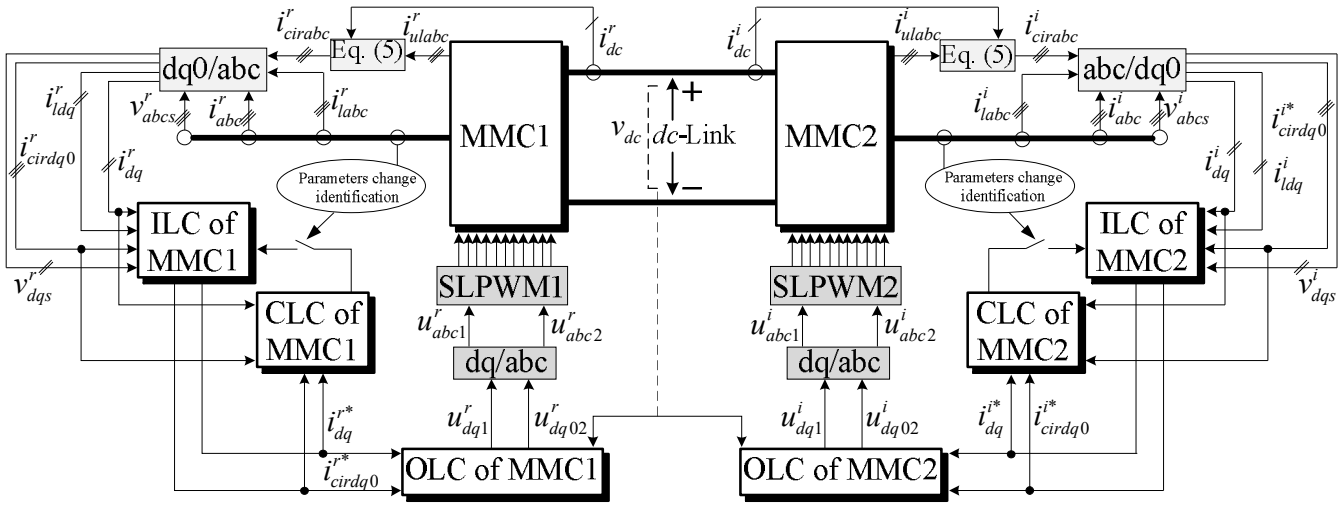


**Fig. 7. Block diagram of the proposed control technique for the MMC-HVDC system in Fig. 1.**

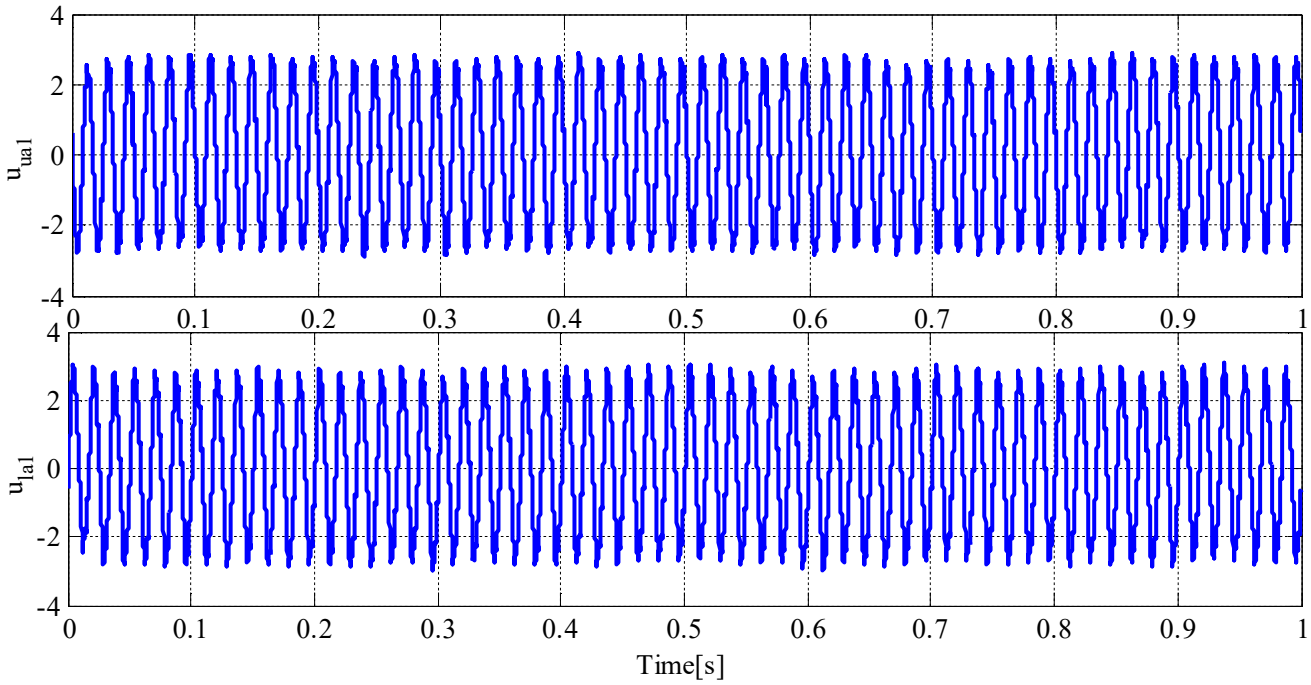


**(a)**

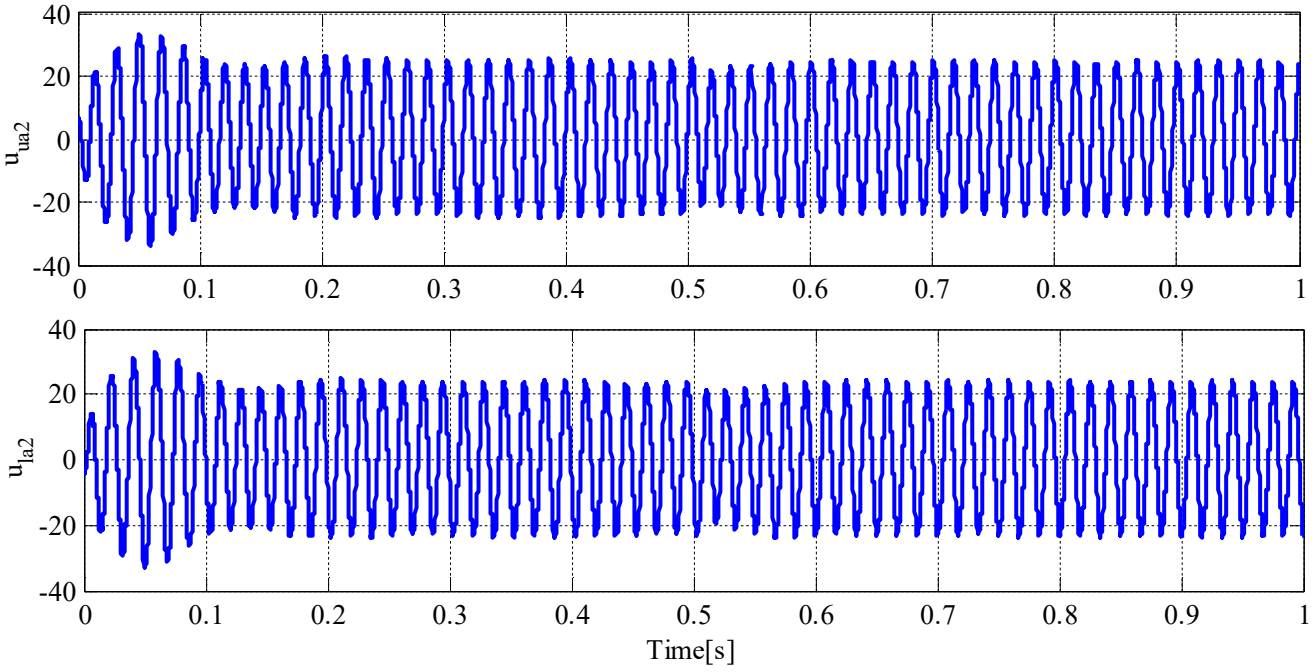


**(b)**

**Fig. 8. The upper and lower switching functions of phase "a' of (a) MMC1 (b) MMC2, under load changes.**

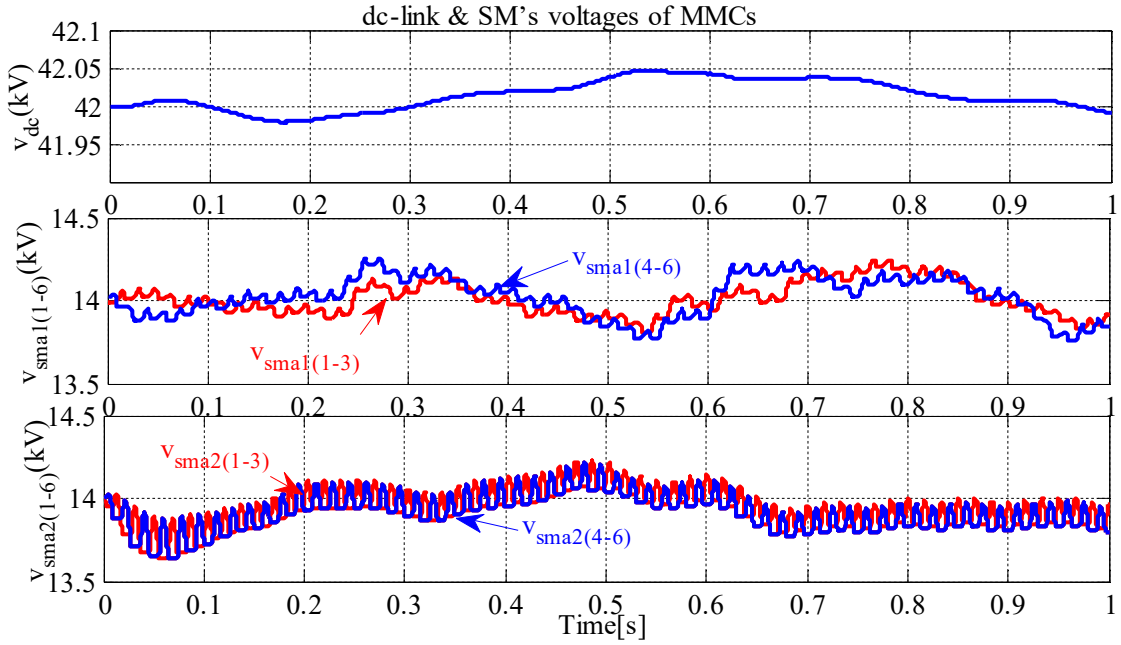


**Fig. 9. MMCs dc-link and Sub-Module's voltages with load changes.**

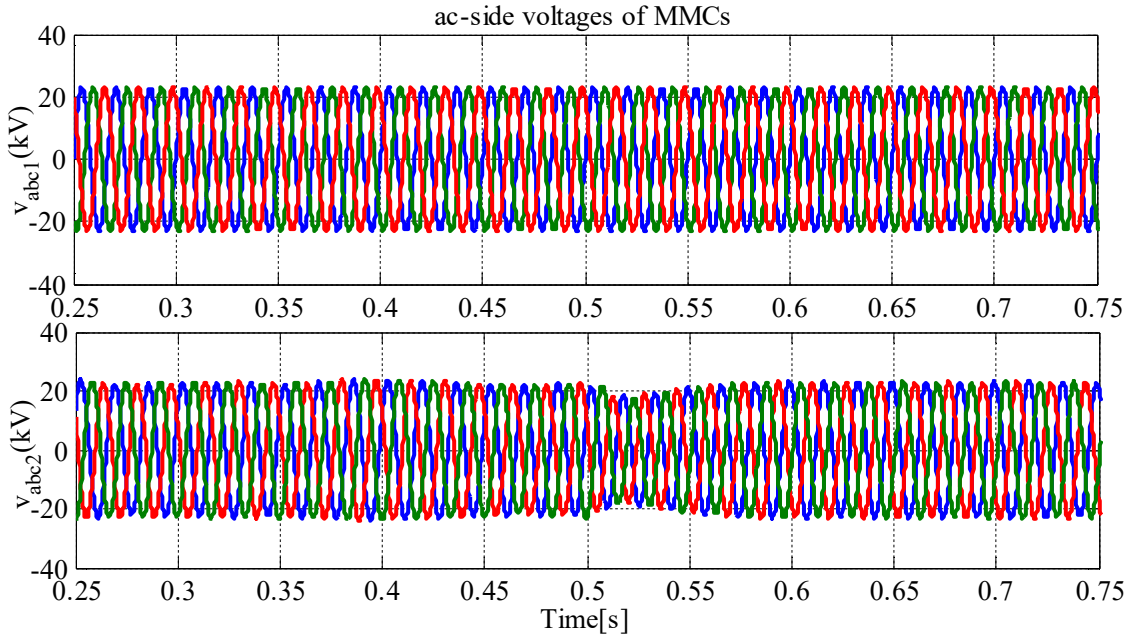


**Fig. 10. MMCs *ac* voltages with load changes.**

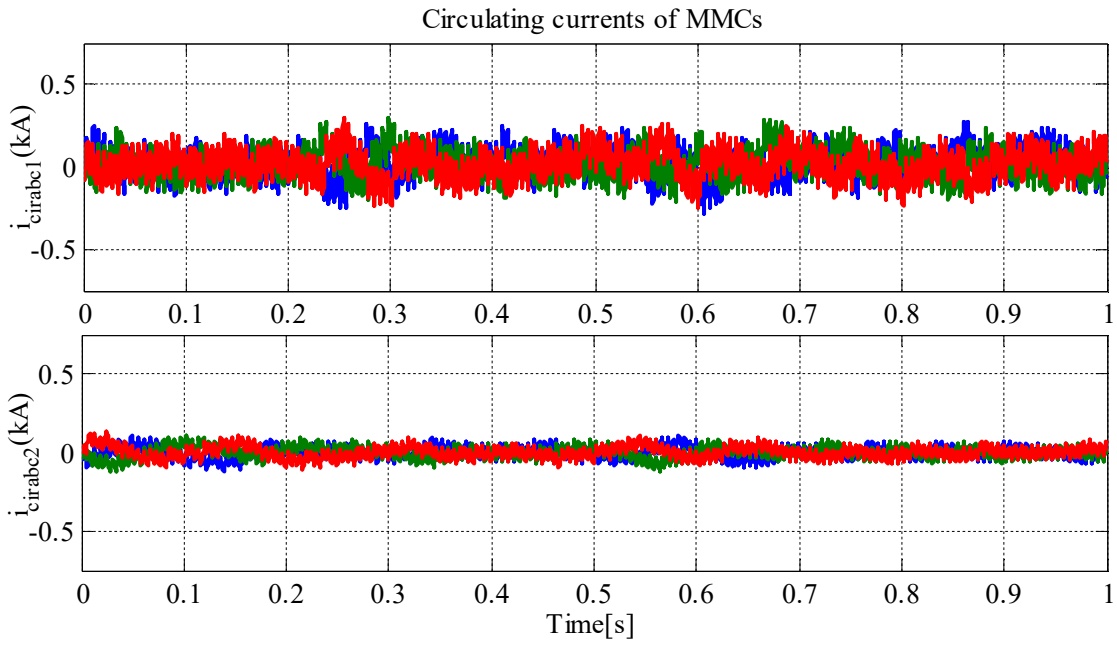


**Fig. 11. MMCs Circulating currents with load changes.**

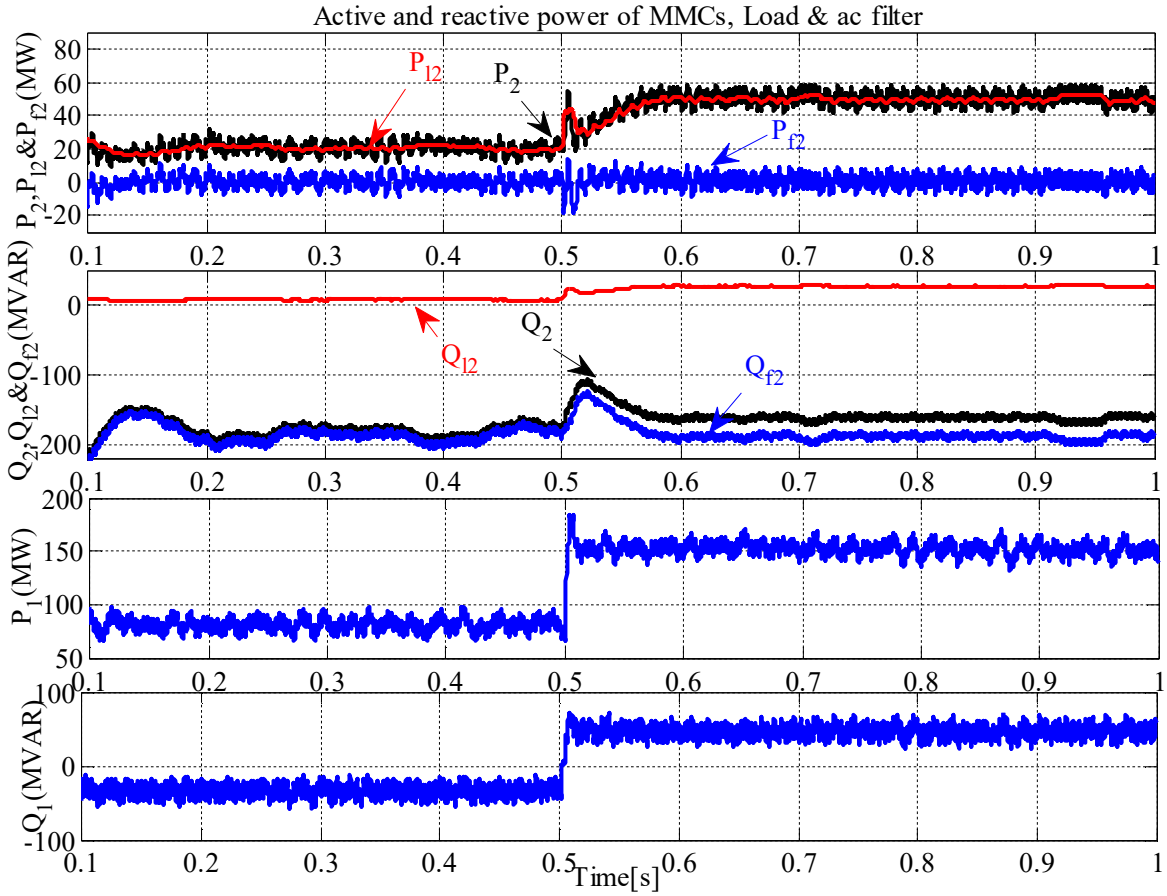


**Fig. 12. Active and reactive power of MMCs, load, and *ac* filter with load changes.**

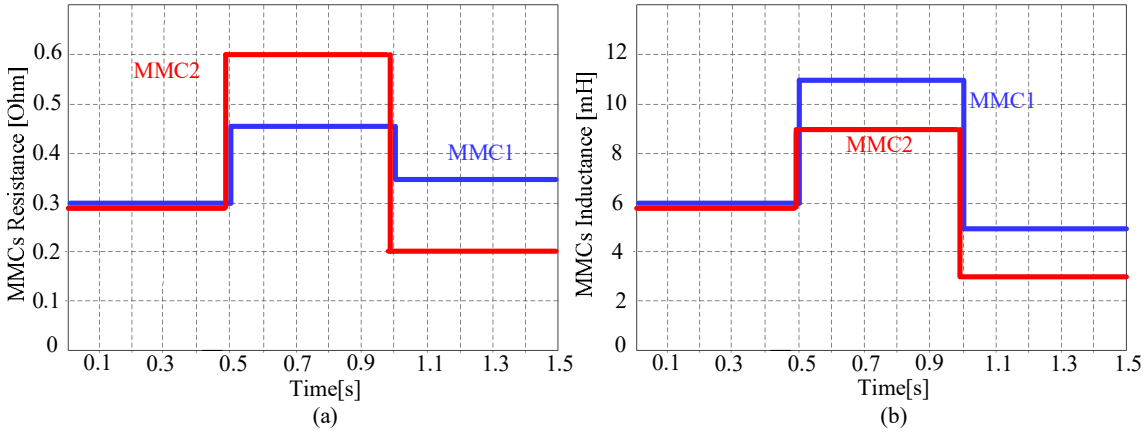


**Fig. 13. Parameters changes for (a) the resistance of MMCs (b) the inductance of MMCs.**

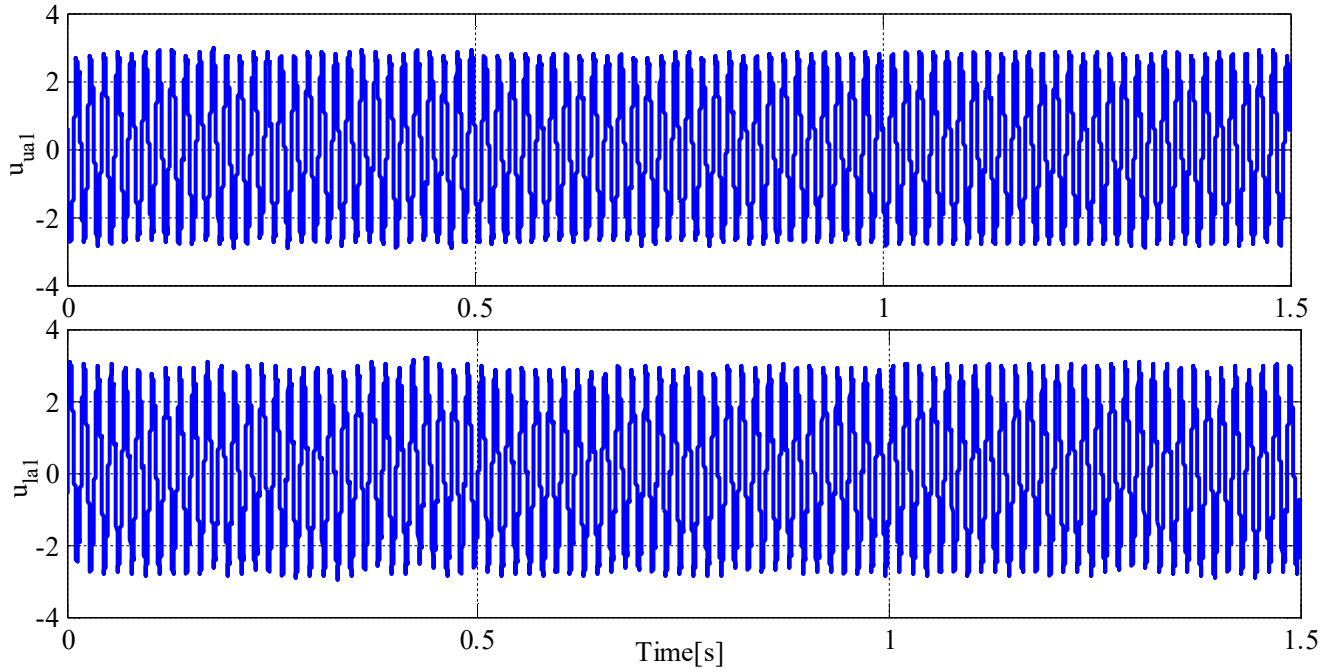


**(a)**

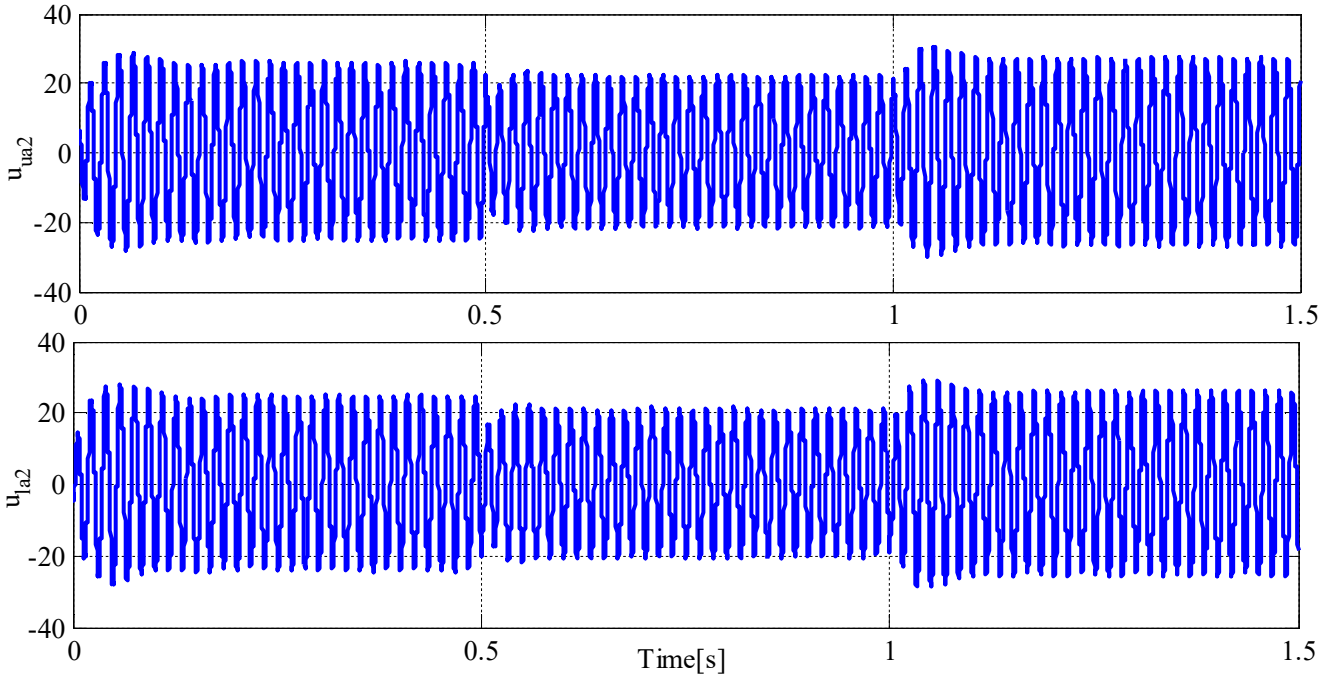


**(b)**

**Fig. 14. The upper and lower switching functions of phase "a'' of (a) MMC1 (b) MMC2, under MMC parameters changes.**

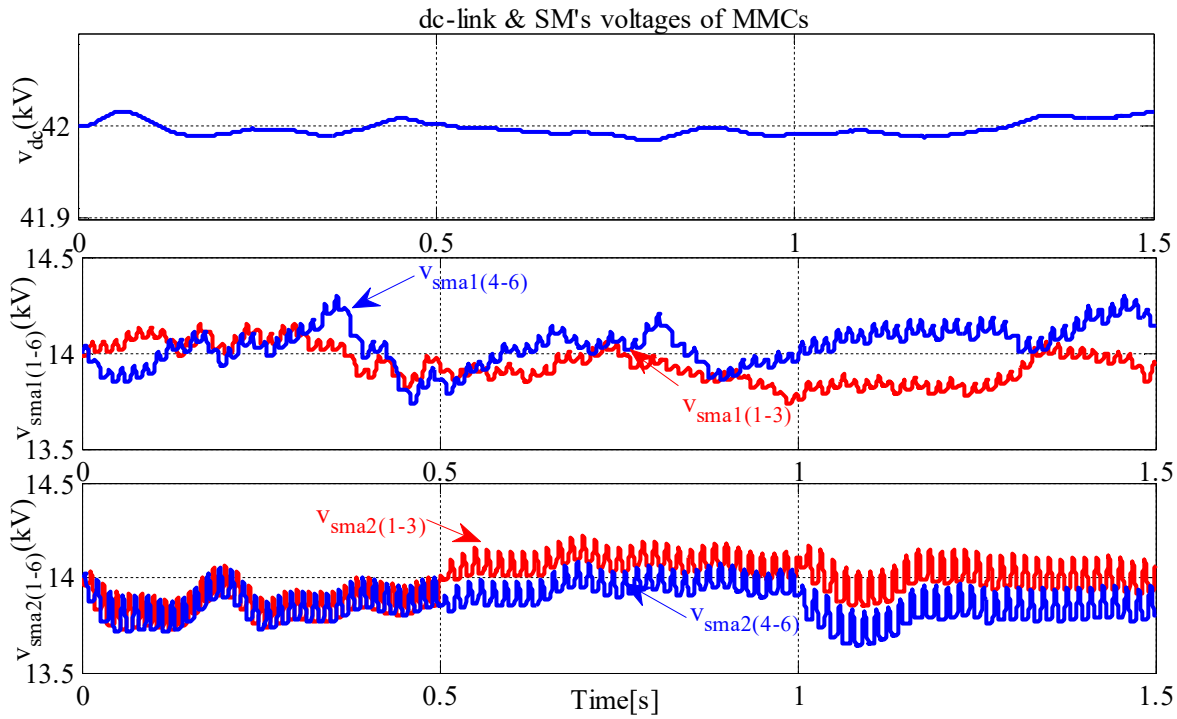


**Fig. 15. MMCs dc-link and SM's voltages with parameters changes.**

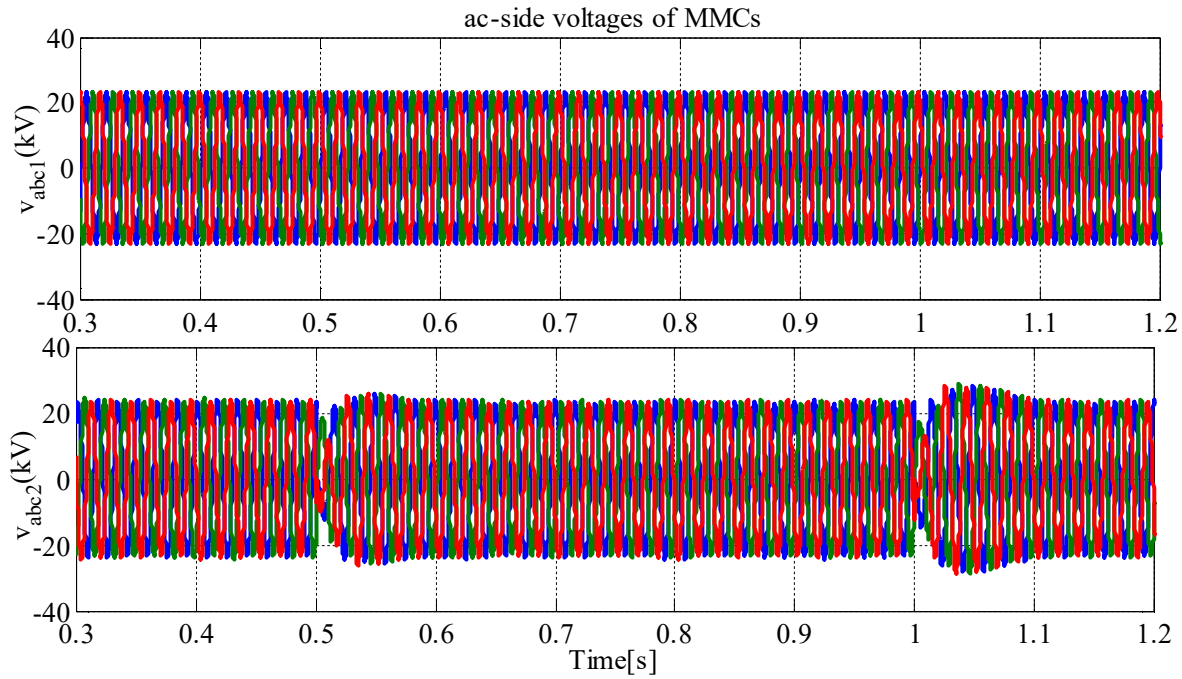


**Fig. 16. MMCs ac voltages with the parameters changes.**

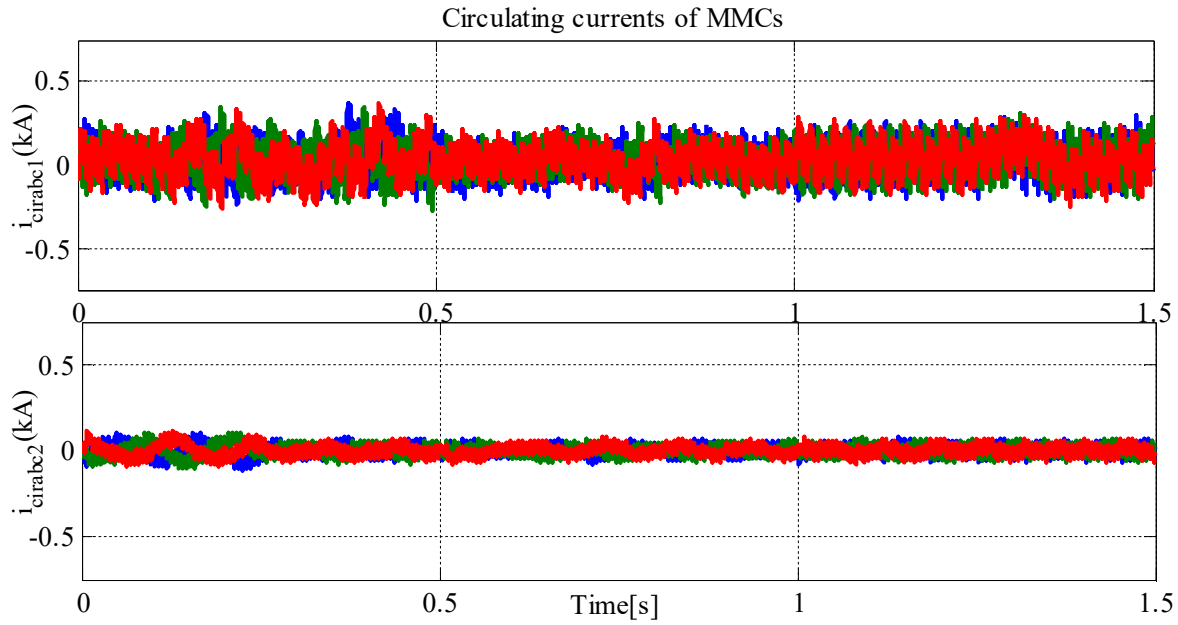


**Fig. 17. MMCs circulating currents with parameters changes.**

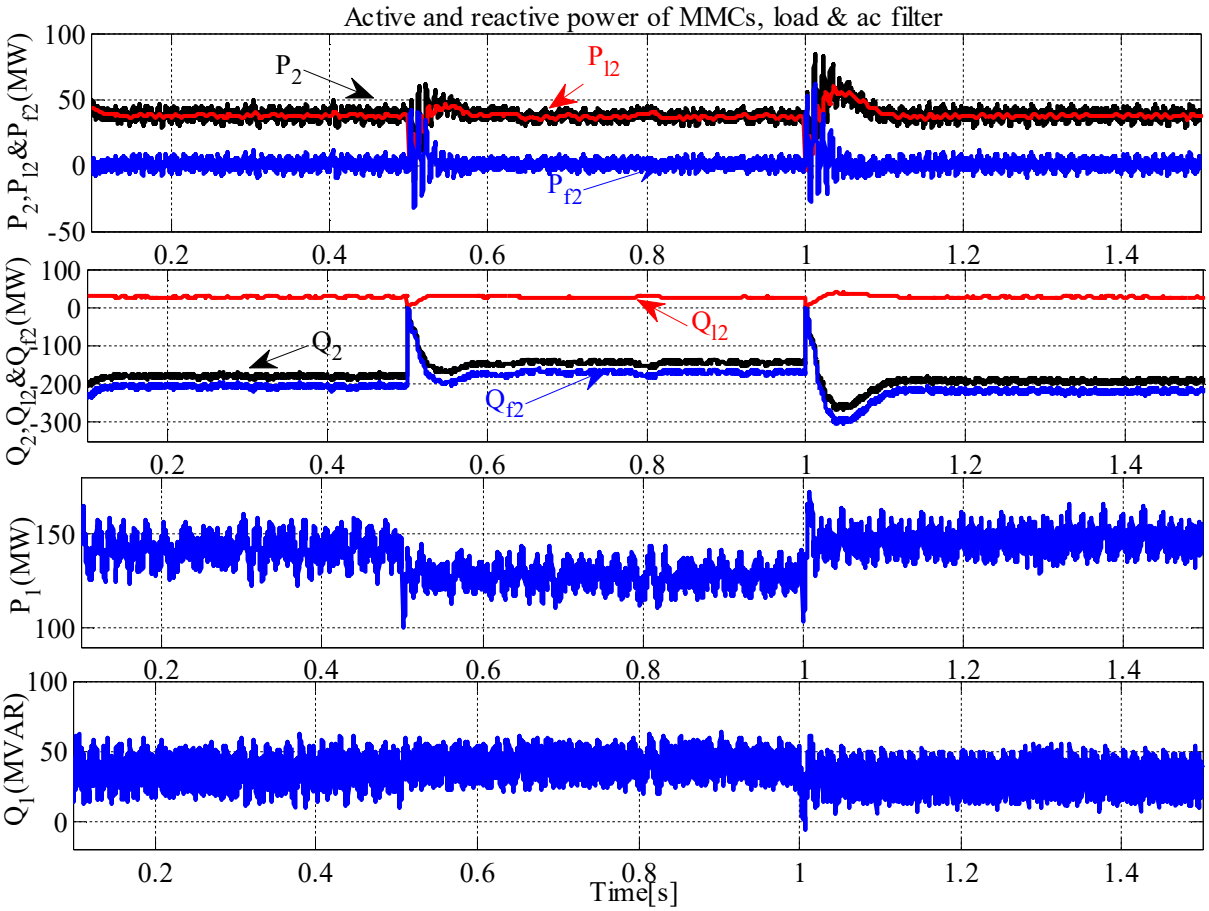


**Fig. 18. Active and reactive power of MMCs, load, and *ac* filter with parameters changes.**